

Asymmetric Modulation of El Niño and La Niña and the Linkage to Tropical Pacific Decadal Variability

YUKO M. OKUMURA, TIANYI SUN, AND XIAN WU

Institute for Geophysics, Jackson School of Geosciences, The University of Texas at Austin, Austin, Texas

(Manuscript received 13 September 2016, in final form 9 March 2017)

ABSTRACT

El Niño–Southern Oscillation (ENSO) in a 1300-yr preindustrial control simulation of the Community Climate System Model, version 4 (CCSM4), exhibits distinct modulation in association with tropical Pacific decadal variability (TPDV). The frequency and duration of El Niño events modulate with changes in the interbasin sea surface temperature (SST) gradient related to the leading mode of TPDV, which resembles the interdecadal Pacific oscillation (IPO). La Niña shows similar changes with the IPO but is also controlled by changes in El Niño that often precedes La Niña, and these effects tend to cancel each other. The amplitude of ENSO, on the other hand, is closely related to the second leading mode of TPDV that affects the zonal and meridional contrast of tropical Pacific climate. Significant changes in the pattern and seasonal evolution related to this TPDV mode are found mainly for El Niño because of the nonlinear relation between the atmospheric deep convection and SSTs. The resultant changes in the amplitude of El Niño, in turn, affect the amplitude and duration of the following La Niña, as well as the asymmetry in their patterns and duration. The decadal ENSO modulation associated with both TPDV modes is not symmetrical between El Niño and La Niña and thus is not likely to occur solely as a result of random variability. The patterns of TPDV in CCSM4 have resemblance to those simulated by its atmospheric component coupled to a slab ocean model, suggesting that TPDV induced by stochastic atmospheric variability interacts with the ENSO dynamics.

1. Introduction

Dynamic and thermodynamic feedbacks between the ocean and atmosphere give rise to the El Niño–Southern Oscillation (ENSO) phenomenon in the equatorial Pacific, the dominant mode of climate variability on interannual time scales (e.g., Wallace et al. 1998; Neelin et al. 1998; Wang and Picaut 2004; Chang et al. 2006). Warm (El Niño) and cold (La Niña) phases of ENSO typically last 1–2 yr and repeat approximately every 3–8 yr. El Niño and La Niña are not a simple mirror image and exhibit asymmetry in their spatial pattern and seasonal evolution (e.g., Hoerling et al. 1997; Burgers and Stephenson 1999; Kessler 2002; Larkin and Harrison 2002; Ohba and Ueda 2009; Okumura and Deser 2010). Changes in the atmospheric deep convection associated with ENSO force an atmospheric Rossby wave into the extratropics, inducing climate anomalies over many parts of the world (e.g., Trenberth et al. 1998; Alexander et al. 2002). The ENSO phenomenon thus

provides an important source of climate predictability in the tropics and beyond.

Analyses of observational data and paleoclimate proxy records show that the amplitude of ENSO varied considerably on decadal–interdecadal time scales in the past (e.g., Trenberth and Shea 1987; Gu and Philander 1995; Wang and Wang 1996; Cobb et al. 2003; D'Arrigo et al. 2005; Li et al. 2011; Emile-Geay et al. 2013). During the twentieth century, interannual variability of ENSO weakened between the 1920s and early 1960s and rapidly intensified in the late 1960s (Fig. 1). Despite sparse SST observations in the equatorial Pacific during the first half of the twentieth century (e.g., Deser et al. 2010a), this ENSO amplitude modulation is remarkably consistent between instrumental data and various paleoclimate reconstructions (McGregor et al. 2013b). The ENSO amplitude inferred from North American tree ring records exhibits 50–90-yr cycles of modulation over the past 1100 yr (Li et al. 2011). In addition to the amplitude, observational analyses suggest that various other properties of ENSO changed around the Pacific-wide climate regime shift in the late 1970s. In particular, the period of ENSO increased (Gu and Philander 1995;

Corresponding author: Dr. Yuko M. Okumura, yukoo@ig.utexas.edu

DOI: 10.1175/JCLI-D-16-0680.1

© 2017 American Meteorological Society. For information regarding reuse of this content and general copyright information, consult the [AMS Copyright Policy](#) (www.ametsoc.org/PUBSReuseLicenses).

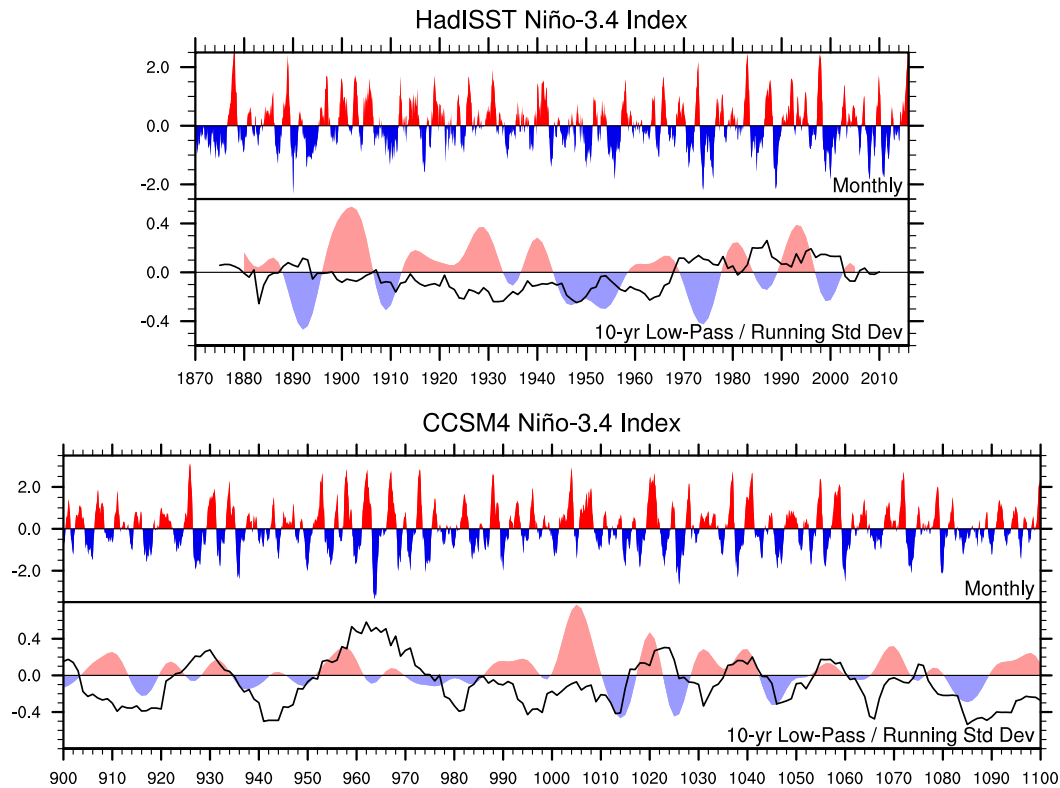


FIG. 1. The Niño-3.4 index ($^{\circ}\text{C}$; dark blue and red shaded curve) and its 10-yr low-pass-filtered component (light blue and pink shaded curve) and 10-yr running standard deviation (black curve) from (top) the HadISST dataset and (bottom) the CCSM4 control simulation for model years 900–1100. The 10-yr running standard deviation is shown as a deviation from the standard deviation for the entire period (0.77°C for HadISST and 1.06°C for CCSM4).

Wang and Wang 1996), El Niño became more frequent than La Niña (Trenberth and Hurrell 1994), propagation direction of sea surface temperature (SST) anomalies associated with El Niño changed from westward to eastward (Wallace et al. 1998; Wang and An 2002; McPhaden and Zhang 2009), and asymmetry in the amplitude and spatial pattern of El Niño and La Niña became more evident (Wu and Hsieh 2003; An 2004). At the same time, background climate shifted toward a more El Niño-like state, with warming in the tropical Pacific and along the west coast of the Americas, cooling in the central North Pacific, and deepening of the wintertime Aleutian low (e.g., Nitta and Yamada 1989; Mantua et al. 1997; Zhang et al. 1997; Garreaud and Battisti 1999; Deser et al. 2004).

The concurrent changes in the background state and ENSO in the late 1970s led to a number of studies investigating the impact of a changing background state on ENSO. Several studies suggest that the present-day ENSO is a neutrally stable mode and a change in the background state affects the stability and properties of this interannual variability (Hao et al. 1993; Jin and Neelin 1993; Fedorov and Philander 2000, 2001).

Indeed, the amplitude and frequency of ENSO are modulated by prescribed mean state changes in accordance with observations in some intermediate or hybrid coupled models (e.g., Wang and An 2002; Ye and Hsieh 2006; Fang et al. 2008; An and Choi 2015). Conversely, it has been argued that ENSO is a stable mode forced by stochastic variability of the atmosphere and its decadal modulation is merely a response to the low-frequency component of noise forcing and hence unpredictable (e.g., Flügel and Chang 1999; Thompson and Battisti 2001; Flügel et al. 2004; Yeh et al. 2004; Wittenberg et al. 2014).

Multicentury simulations of full-physics climate models show that the decadal modulation of ENSO is closely related to changes in the background state, suggestive of their interactions (e.g., Timmermann 2003; Rodgers et al. 2004; Yeh and Kirtman 2004; Choi et al. 2009, 2013; Ogata et al. 2013). In these models, stronger ENSO is associated with a weaker zonal gradient of the background SST and thermocline in the equatorial Pacific (i.e., warmer SST and deeper thermocline in the east and colder SST and shallower thermocline in the west). This zonal dipole pattern emerges as one of

the leading modes of tropical Pacific decadal variability (TPDV) in climate models and is distinct from the zonally symmetric pattern associated with the regime shift or interdecadal Pacific oscillation (IPO; Power et al. 1999). A similar zonal dipole pattern of decadal SST variability is suggested in the analysis of observed SSTs (Sun and Yu 2009; Newman et al. 2016). Yeh and Kirtman (2004) show that the IPO simulated in their model is uncorrelated with the ENSO amplitude, consistent with a recent multimodel study (Choi et al. 2013) and observational analysis (Yeh and Kirtman 2005; McGregor et al. 2010). (Recall that the ENSO amplitude begins to increase in the late 1960s, a decade before the regime shift in Fig. 1.) Despite a number of studies that examine the relation between the late 1970s regime shift and ENSO, it remains ambiguous if the IPO is associated with any other systematic changes in ENSO.

The mechanisms of decadal ENSO modulation and its relation to TPDV are not fully understood. During the period of strong ENSO, the warmer SST in the eastern equatorial Pacific is suggested to enhance positive atmospheric feedback by increasing the sensitivity of the atmospheric deep convection to a given SST anomaly (Choi et al. 2009), while the reduced zonal and vertical gradients of ocean temperatures weaken positive oceanic feedback (Timmermann 2003; Rodgers et al. 2004). A change in ENSO variability may, on the other hand, induce nonzero residual effect on the mean SSTs (Jin et al. 2003; Rodgers et al. 2004; Choi et al. 2009, 2012; Ogata et al. 2013). The strong ENSO acts to increase the mean SSTs in the east and to decrease the mean SSTs in the west because of the eastward displacement of the positive SST anomalies during El Niño compared to the negative ones during La Niña, as well as to the nonlinearity in oceanic processes. Thus, ENSO may serve to reduce the time-mean thermal contrast of the tropical Pacific (Schopf and Burgman 2006; Sun and Zhang 2006). The insufficient knowledge of ENSO modulation mechanisms may be in part responsible for the lack of consensus on the future ENSO behavior in a changing climate (e.g., Guilyardi 2006; Collins et al. 2010; DiNezio et al. 2012; Cai et al. 2015; Zheng et al. 2016; An and Choi 2015).

The limited understanding of TPDV further hampers the studies of decadal ENSO modulation [see Liu (2012) for a review]. Earlier studies of the ENSO modulation associated with IPO consider its linkages to the extratropical ocean and atmosphere. Gu and Philander (1997) and Zhang et al. (1998), among others, propose that decadal changes in the extratropical ocean temperatures are subducted and advected equatorward along isopycnal surfaces, affecting the thermal structure

of the equatorial Pacific and ENSO. Subsequent studies, however, demonstrate that the decadal variations of the tropical Pacific are mostly forced by changes in local winds (Schneider et al. 1999a,b; Hazeleger et al. 2001; Karspeck and Cane 2002). Regarding the atmospheric bridge, Barnett et al. (1999) and Pierce et al. (2000) propose that the low-frequency components of stochastic atmospheric variability in the extratropics affect equatorial winds via changes in subtropical SSTs and resultant changes in the equatorial thermocline modulate ENSO. Note that this mechanism involves changes in the tropical Pacific mean state and thus differs from the null hypothesis of decadal ENSO modulation (e.g., Flügel and Chang 1999).

The stochastic origin of TPDV has been revisited by recent studies (Dommenges and Latif 2008; Dommenges 2010; Clement et al. 2011; Okumura 2013). These studies show that atmospheric models coupled to a mixed layer ocean can generate ENSO-like low-frequency variability although most models do not reproduce the observed interannual spectral peak, for which ocean dynamics plays an important role. The TPDV simulated in these models may have its origin in the extratropics (Dommenges and Latif 2008; Okumura 2013), in agreement with the earlier studies by Barnett et al. (1999) and Pierce et al. (2000). Okumura (2013) discusses that the tropical Pacific Ocean is more strongly affected by stochastic atmospheric forcing from the South Pacific than from the North Pacific as a result of the northward displacement of the intertropical convergence zone (ITCZ), which is supported by coupled model experiments by Zhang et al. (2014b). Yeh and Kirtman (2004) show that the IPO is indeed of stochastic origin in a series of coupled model experiments where a single ocean model is coupled to various numbers of atmospheric models to control the amplitude of atmospheric noise. However, they suggest that a damped, stochastically forced process cannot readily explain the decadal variability linked to the ENSO amplitude.

The interactions between stochastically generated TPDV and ENSO dynamics may be the key to understand both TPDV and ENSO modulation (Burgman et al. 2008). Building on this concept, the present study aims to address several unsolved issues regarding the linkage between TPDV and ENSO modulation through analyses of a long control climate model simulation. While previous studies of decadal ENSO modulation focus on the ENSO amplitude, we analyze how various other properties of ENSO change with TPDV. In particular, we investigate if there are any systematic changes in ENSO other than the amplitude in association with the IPO. The mechanisms of decadal changes in ENSO properties are explored through various

analyses of ocean–atmosphere fields. The analyses are conducted separately for El Niño and La Niña given the asymmetric nature of their spatial patterns and temporal evolution. A hypothesis arising from the climate model analyses is also tested through experiments with an atmospheric model. Finally, to understand the origins of TPDV and its interactions with the ENSO dynamics, the patterns of TPDV simulated in a climate model are compared with those in a control simulation of its atmospheric component coupled to a slab ocean model.

The rest of the paper is organized as follows. [Section 2](#) describes the models and analysis methods used in this study. [Section 3](#) gives an overview of ENSO modulation and its relation to TPDV and then analyzes the mechanisms of modulation in various ENSO properties. The origins of TPDV and the feedback from ENSO modulation are discussed in [section 4](#). The summary and concluding remarks are given in [section 5](#).

2. Models and methods

a. CCSM4 control simulation

In this study, we mainly analyze a 1300-yr pre-industrial control simulation of the Community Climate System Model, version 4 (CCSM4; [Gent et al. 2011](#)). The CCSM4 is a state-of-the-art climate model developed at the National Center for Atmospheric Research and comprising four components (atmosphere, ocean, land, and cryosphere) linked by means of a flux coupler. The atmospheric component, the Community Atmosphere Model, version 4 (CAM4), uses a finite-volume dynamical core and has a horizontal resolution of 0.9° latitude and 1.25° longitude with 26 levels in the vertical. The oceanic component has longitudinal spacing of 1.13° and latitudinal spacing varying from 0.27° at the equator to 0.65° at 60°N , with 60 levels in the vertical. The radiative forcing is kept at the 1850 level in the control simulation. The SST and upper-ocean heat content show very small drifts in the tropical oceans throughout the simulation, and thus we use the whole 1300-yr data for our analyses. The long simulation ensures stable statistics. For example, a correlation coefficient that exceeds 0.1 in absolute value is significantly different from 0 at the 99% confidence level in one-sided correlation analysis of yearly anomalies (approximate sample size of ~ 650 ; cf. [Figs. 6 and 7](#)).

The CCSM4 displays notable improvements in simulating salient features of tropical Pacific climate and its variability on seasonal–decadal time scales compared to its predecessor CCSM3, owing mainly to changes in the atmospheric deep convection scheme ([Neale et al. 2008](#);

[Gent et al. 2011](#); [Danabasoglu et al. 2012](#); [Deser et al. 2012](#)). Compared to CCSM3, the spatial pattern and seasonal evolution of ENSO events became more realistic and the period lengthened from 2 to 3–6 yr in CCSM4. In particular, the pattern and duration of El Niño and La Niña simulated in CCSM4 exhibit asymmetry as in observations ([Fig. 2](#)): SST, surface wind, precipitation, and sea surface height (SSH) anomalies associated with El Niño are displaced eastward compared to those for La Niña, and El Niño tends to terminate quickly after peaking toward the end of the calendar year, while La Niña often persists into the following year and reintensifies in boreal winter. Importantly, the CCSM4 simulates the decadal modulation of ENSO amplitude, although the overall amplitude is larger by about 30% in CCSM4 compared to observations ([Fig. 1](#)). Despite the excessively strong ENSO, the amplitude of TPDV simulated in CCSM4 is comparable to that in observations over the Niño-3.4 region.

A 2200-yr control simulation of the newer version of the model [the Community Earth System Model, version 1 (CESM1; [Kay et al. 2015](#))] is also available, and this model simulates a more realistic amplitude of ENSO. The CESM1, however, has larger cold SST bias in the equatorial Pacific compared to CCSM4, and the equatorial precipitation has muted response to ENSO. In addition, El Niño events simulated in this model have a tendency to last 2 yr and to intensify in the second year ([DiNezio et al. 2017](#)), which is rare in observations. For these reasons, we elect to analyze the CCSM4 control simulation. Detailed analyses of the ENSO modulation in CESM1 and other climate models are reserved for future studies.

b. ENSO and TPDV

We define El Niño and La Niña events when monthly SST anomalies averaged in the Niño-3.4 region (5°S – 5°N , 170°W – 120°W ; here called the Niño-3.4 index) in December exceed one standard deviation (1.27°C) or are below minus one standard deviation (-1.27°C), respectively. The first year when the Niño-3.4 index satisfies this criterion is set as year 0, and the months of that year are noted as $\text{Jan}^0, \text{Feb}^0, \dots, \text{Dec}^0$. If the Niño-3.4 index satisfies the criterion in consecutive years, it is counted as a single event. There are a total of 193 El Niño events and 180 La Niña events in the 1300-yr CCSM4 control simulation. Monthly standard deviations of the Niño-3.4 index peak in January in CCSM4 instead of December in observations ([Deser et al. 2012](#)), but we use the December index to define ENSO events in CCSM4 for the consistency with observational analysis (e.g., [Okumura and Deser 2010](#)).

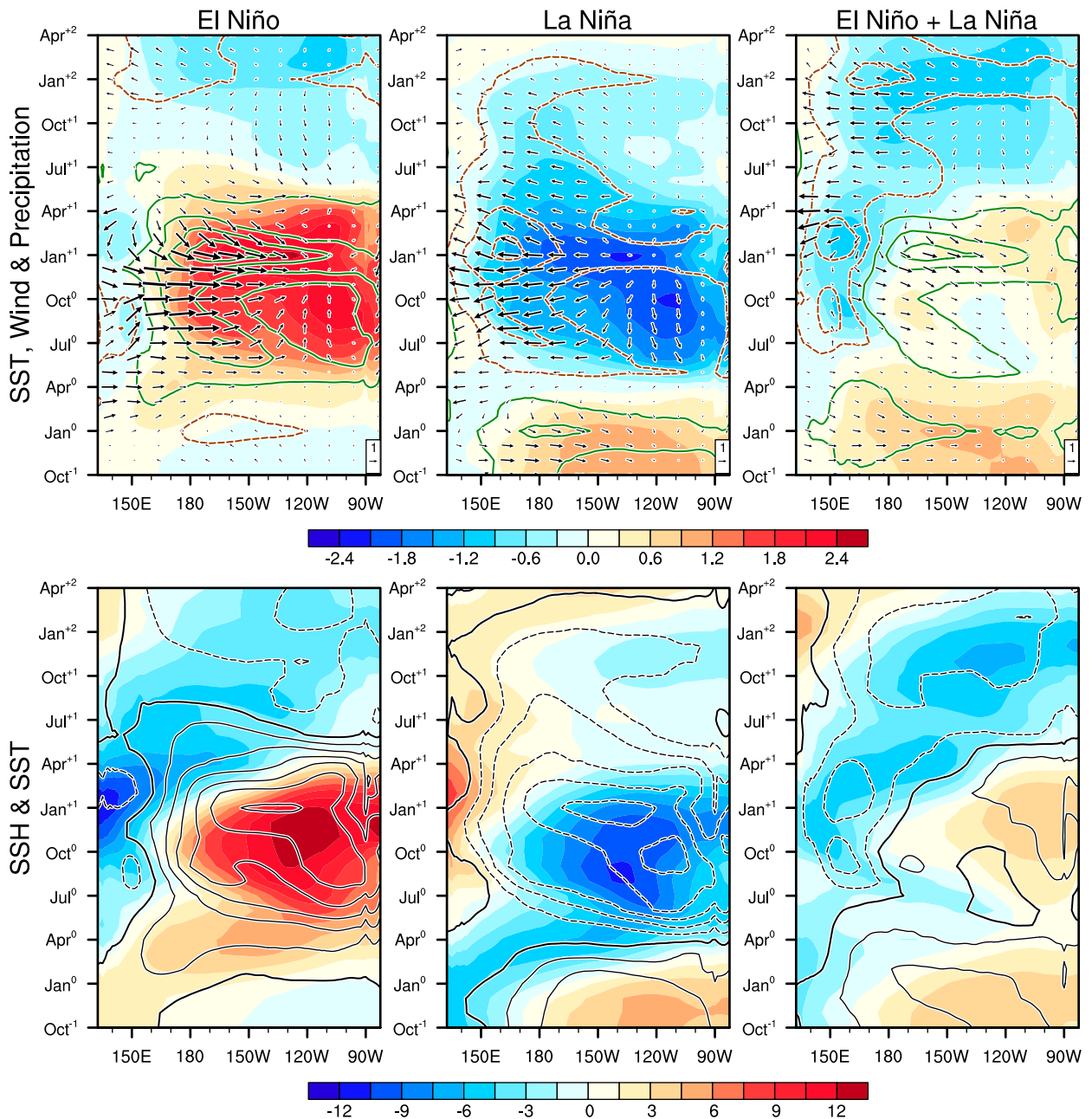


FIG. 2. Longitude–time cross sections of composite (top) SST ($^{\circ}\text{C}$; shading), surface wind (m s^{-1} ; vectors), and precipitation [positive (negative) contours in green solid (brown dashed) at $\pm 1, 3, 5, \dots \text{mm day}^{-1}$] and (bottom) SSH (cm; shading) and SST (black contours at intervals of 0.4°C ; zero contours thickened) anomalies along the equator (3°S – 3°N) for Oct⁻¹–Apr⁺² of (left) El Niño and (center) La Niña events in the CCSM4 control simulation and (right) sum of (left) and (center).

Using the January index instead does not affect the results of this study.

The leading modes of TPDV are defined based on empirical orthogonal function (EOF) analysis of 10-yr low-pass-filtered annual SSTs in the tropical Pacific (20°S – 20°N , 120°E – 80°W). The two leading modes combined explain 71% of the total low-pass-filtered variance in CCSM4 (Fig. 3). The global regression map based on the

leading principal component (PC1) resembles the IPO in observations and shows zonally symmetric warming in the tropical Pacific and cooling in the central North Pacific for the positive phase, with associated changes in tropical precipitation and extratropical atmospheric circulation. The regression map based on PC2, on the other hand, shows a zonal dipole pattern in tropical Pacific SST and precipitation and a meridional displacement of the ITCZ

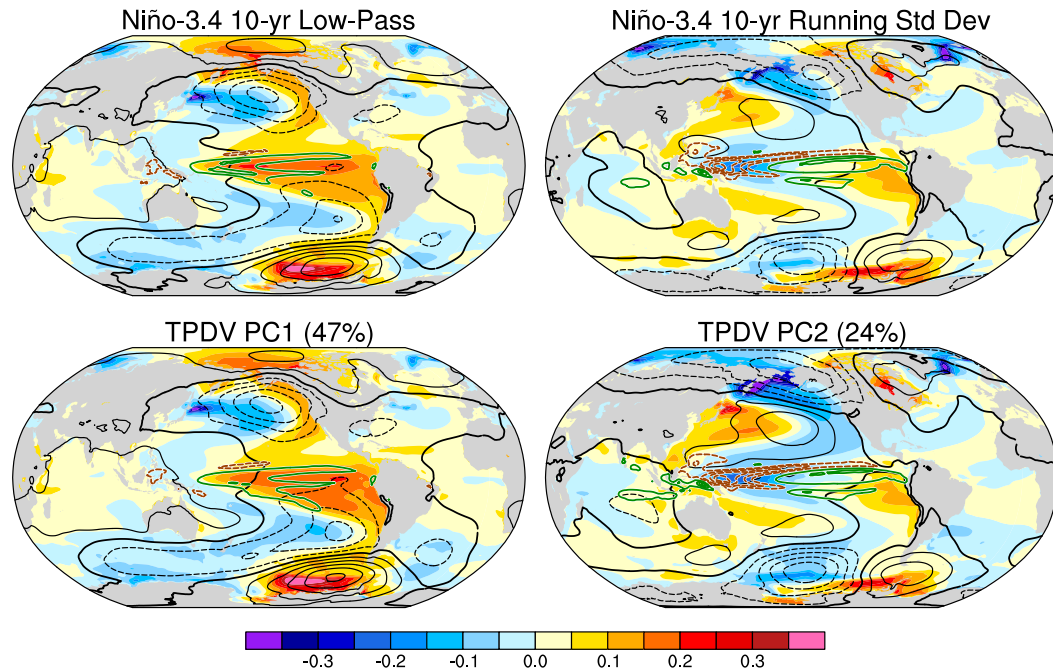


FIG. 3. Regression maps of global SST ($^{\circ}\text{C}$; shading), SLP (black contours at intervals of 0.1 hPa; zero contours thickened), and precipitation [positive (negative) contours in green solid (brown dashed) at intervals of 0.2 mm day^{-1}] anomalies on (top) (left) the 10-yr low-pass-filtered component and (right) 10-yr running standard deviation of the Niño-3.4 index and (bottom) the (left) PC1 and (right) PC2 of TPDV in the CCSM4 control simulation. The predictors are standardized and SST, SLP, and precipitation data are smoothed with a 10-yr low-pass filter prior to the regression analysis. The first and second modes of TPDV explain 47% and 24% of the total low-pass-filtered variance, respectively.

in the eastern equatorial Pacific. These patterns of TPDV are similar to those simulated in other climate models (e.g., Yeh and Kirtman 2004).

We analyze how various properties of ENSO change with the two leading modes of TPDV in the CCSM4 control simulation. The analyses of El Niño and La Niña events are conducted separately for the positive and negative phases of the two TPDV modes. Given the potential interactions of ENSO and TPDV, it is difficult to strictly distinguish ENSO from TPDV in a moving time frame. The analyses presented in the paper are based on the ocean–atmosphere anomalies defined as deviations from the climatology for the entire 1300-yr simulation, but we repeat all the analyses by using 10-yr high-pass-filtered anomalies and confirm that the main results do not depend on the data processing unless stated otherwise.

As mentioned earlier, the CCSM4 reproduces the observed asymmetry in the pattern and duration of El Niño and La Niña. Previous studies suggest that the ENSO asymmetry results from the nonlinearity in the tropical ocean–atmosphere system, especially the nonlinear relations between the atmospheric deep convection or wind and SSTs (Hoerling et al. 1997; Kang and Kug 2002; Ohba and Ueda 2009; Wu et al. 2010; Okumura et al. 2011; Dommenges et al. 2013; McGregor

et al. 2013a) and between the thermocline depth and SSTs (Burgers and Stephenson 1999; Meinen and McPhaden 2000; Galanti et al. 2002; DiNezio and Deser 2014). These nonlinear processes may also affect the way by which ENSO interacts with TPDV. The present study shows that this is indeed the case, and thus all the analyses presented in the paper are conducted separately for El Niño and La Niña.

c. CAM4-SOM control simulation

To understand the origins of TPDV, the CCSM4 control simulation is compared to a 500-yr control simulation of CAM4 coupled to a slab ocean model (SOM). The SOM has the same horizontal grid as CAM4 and computes SSTs from surface heat flux and Q flux, which represents the effect of climatological ocean heat transport. The CAM4-SOM also includes the same land and sea ice models as CCSM4. The ocean and atmosphere are only thermodynamically coupled in this model, and therefore the Bjerknes feedback is absent. The mixed layer depth and Q flux are based on the climatology of the CCSM4 control simulation. The Q flux varies monthly, but the mixed layer depth is fixed at the annual mean value to better balance the annual cycle of heat (Bailey et al. 2009). The fixed mixed layer depth

results in larger SST variability over the extratropical oceans compared to CCSM4, as the mixed layer does not deepen in winter when atmospheric variability intensifies (not shown). The leading modes of TPDV in CAM4-SOM are defined using the same method for CCSM4 (section 2b). Okumura (2013) compares the leading mode of TPDV in CCSM4 and CAM4-SOM. In this study, we extend the analysis to the second leading mode of TPDV and discuss the role of stochastic atmospheric forcing and equatorial ocean dynamics.

d. CAM4 experiments

The analyses of the CCSM4 control simulation suggest that the second leading mode of TPDV has asymmetric impacts on the seasonal evolution of El Niño and La Niña. To test if this asymmetry arises from nonlinearity in the atmosphere, we conduct standalone CAM4 experiments. Two sets of El Niño and La Niña experiments are conducted by prescribing composite monthly SSTs from Jan⁰ to December of the third year (Dec⁺²) based on the CCSM4 control simulation. In the first and second sets of El Niño and La Niña experiments, we add time-invariant background SST changes associated with the positive and negative phases of the second leading mode of TPDV, respectively. The TPDV SST anomaly pattern is derived by regressing 10-yr low-pass-filtered annual mean SSTs on one standard deviation PC2 (Fig. 3). Each of these four experiments consists of 20-member ensemble simulations initialized with different atmospheric conditions. The ensemble-mean atmospheric response in each experiment is compared with the climatology of a 300-yr CAM4 control simulation forced with monthly SST climatology from the CCSM4 control simulation.

3. Results

a. TPDV and ENSO modulation

The CCSM4 control simulation displays distinct modulation of ENSO on decadal–interdecadal time scales throughout the 1300-yr integration. Figure 1 shows the monthly Niño-3.4 index from a 200-yr segment of the CCSM4 simulation and the Hadley Centre Sea Ice and SST (HadISST) dataset for 1870–2016 (Rayner et al. 2003). The amplitude of interannual ENSO variability fluctuates considerably from decade to decade in CCSM4, as quantified by 10-yr running standard deviations of the Niño-3.4 index. The running standard deviations range from 0.52° to 1.65°C, changes that are more than 50% of the overall amplitude of 1.06°C. These values are significantly larger than those in observations (the range of running standard deviations from 0.51° to 1.03°C and the overall amplitude of 0.77°C). In agreement with previous studies (Yeh and

Kirtman 2004, 2005; McGregor et al. 2010), the modulation of ENSO amplitude is barely correlated with the decadal variations of the Niño-3.4 index in both CCSM4 ($r = 0.01$) and observations ($r = -0.17$), which are associated with the IPO in observations.

The decadal variations of the Niño-3.4 index in CCSM4 are also associated with a Pacific-wide anomaly pattern that resembles the observed IPO (Fig. 3). This pattern emerges as the leading mode of TPDV that explains nearly half of the total low-pass-filtered variance in the CCSM4 simulation. Indeed, the decadal component of Niño-3.4 index and PC1 of TPDV are highly correlated at $r = 0.95$. The decadal modulation of the ENSO amplitude in CCSM4, on the other hand, is associated with a zonal dipole pattern of SST and precipitation anomalies in the tropical Pacific (Fig. 3), consistent with previous modeling studies. This pattern is closely related to the second leading mode of TPDV that explains 24% of the total low-pass-filtered variance in the CCSM4 simulation. The ENSO amplitude and PC2 of TPDV are correlated at $r = 0.81$. During the decades of enhanced ENSO, SSTs and precipitation increase in the east and decrease in the west, weakening their climatological zonal contrast. In the eastern tropical Pacific, precipitation anomalies also show a meridional dipole pattern, indicative of a meridional displacement of the ITCZ. This meridional dipole pattern of precipitation anomalies is most pronounced in boreal summer–fall when the climatological cold tongue develops in the equatorial Pacific (not shown). The ocean–atmosphere anomalies associated with the ENSO amplitude modulation are not limited to the tropical Pacific but extend well into the extratropics. SLP anomalies show a north–south dipole pattern similar to the North Pacific Oscillation (NPO; Rogers 1981) in the North Pacific and a wave train pattern similar to but in quadrature with the Pacific–South American pattern (PSA2; Mo 2000) in the South Pacific, with associated extratropical SST anomalies. The second leading mode of TPDV is not correlated with the leading mode of TPDV at any lags ($r < 0.1$), while their lagged relationship is reported in a previous study (Choi et al. 2012). Several previous studies also suggest the linkage between ENSO amplitude modulation and Atlantic multidecadal variability (Dong et al. 2006; Timmermann et al. 2007; Kang et al. 2014), but they are not significantly correlated in the CCSM4 control simulation.

Do any properties of ENSO other than the amplitude vary with the two leading modes of TPDV in CCSM4? Figure 4 shows the temporal evolution of Niño-3.4 index for individual and composite El Niño and La Niña events that occur during the positive and negative phases of the two TPDV modes. The most striking

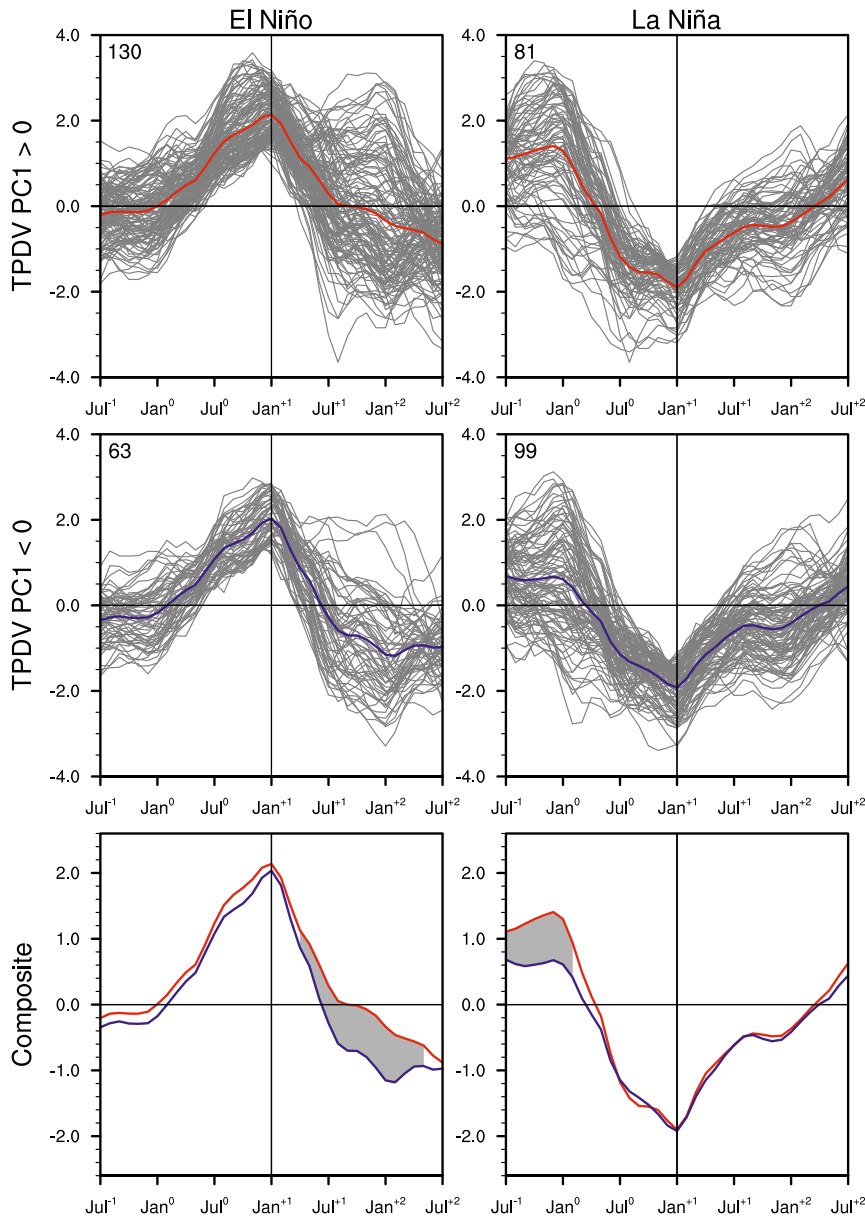


FIG. 4. Time series of the Niño-3.4 index ($^{\circ}\text{C}$) from Jul^{-1} to Jul^{+2} for (left) El Niño and (right) La Niña events that occur during the (top) positive and (middle) negative phases of the PC1 and PC2 TPDV modes in the CCSM4 control simulation. The time series for individual and composite events are shown by thin gray and thick colored curves, respectively. The number of events is shown at the top-left corner. (bottom) Comparison of the composite time series for the positive (red) and negative (blue) phases of TPDV. Gray shading indicates where the difference between the two composites is statistically significant at the 99% confidence level.

change associated with the first mode of TPDV (i.e., the simulated IPO) is the frequency of El Niño events. During the positive phase of IPO, the frequency of El Niño doubles compared to the negative phase. The frequency of La Niña, on the other hand, becomes larger during the negative than the positive phase of IPO, but the difference is not as striking as the El Niño

change. These asymmetric changes in the frequency of El Niño and La Niña may be related to the asymmetry in their onset mechanisms. Consistent with observations, many La Niña events are preceded by El Niño events in the CCSM4 simulation, while El Niño events tend to develop from a neutral condition (Table 1). During the negative phase of IPO, the number of La

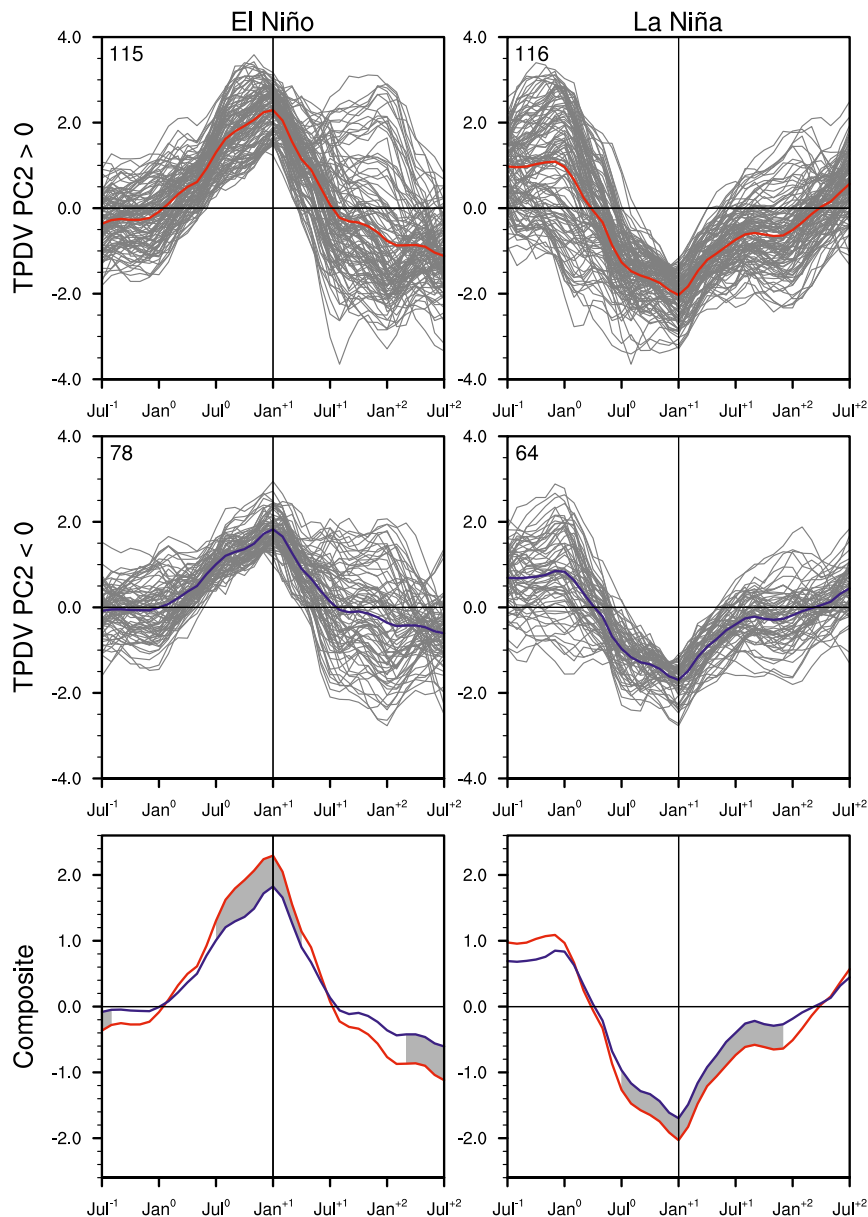


FIG. 4. (Continued)

Niña that develop from a neutral condition increases, but this change is largely counteracted by a decrease in the number of La Niña that follows El Niño. When the 10-yr high-pass-filtered Niño-3.4 index is used for the analysis, these two effects nearly cancel out, and the frequency of La Niña does not change significantly between the positive and negative phases of IPO. (The latter effect becomes slightly larger than the first effect, and the frequency of La Niña decreases negligibly during the negative phase of IPO.) This result is not inconsistent with observational and paleoclimate studies that suggest IPO-related changes in the relative frequency of El Niño

and La Niña events [Kiem et al. 2003; Verdon and Franks 2006; see also a model study by Power et al. (2006)].

Another significant ENSO change associated with the IPO is the duration of El Niño events (Figs. 4 and 5). Most El Niño events that last more than a year after Dec⁰ occur during the positive phase of IPO. It is noteworthy that the two longest El Niño events in observational record (1939–42 and 1991–95) occurred during the positive phase of IPO. There is no systematic difference in the duration of La Niña events associated with the IPO. The increased duration of El Niño events during the positive phase of IPO causes a warm bias in the composite evolution of the

TABLE 1. The number of El Niño (La Niña) events and those preceded by La Niña (El Niño) or neutral conditions in December of the prior year (year -1) for the entire CCSM4 control simulation (first row) and during the positive and negative phases of the leading TPDV mode (second and third rows). The numbers in parentheses are based on the 10-yr high-pass-filtered Niño-3.4 index.

	Year -1			Year -1		
	El Niño	La Niña	Neutral	La Niña	El Niño	Neutral
All years	193 (194)	7 (10)	186 (184)	180 (181)	78 (83)	102 (98)
TPDV PC1 > 0	130 (123)	4 (6)	126 (117)	81 (93)	46 (51)	35 (42)
TPDV PC1 < 0	63 (71)	3 (4)	60 (67)	99 (88)	32 (32)	67 (56)

Niño-3.4 index in year 1 compared to the negative phase (Fig. 4). The composite evolution of the Niño-3.4 index also confirms that La Niña events tend to be preceded more by El Niño events in the previous year during the

positive phase of IPO compared to the negative phase. There is no other significant difference in the timing and amplitude of both El Niño and La Niña events related to the IPO as revealed by the analysis of the Niño-3.4 index.

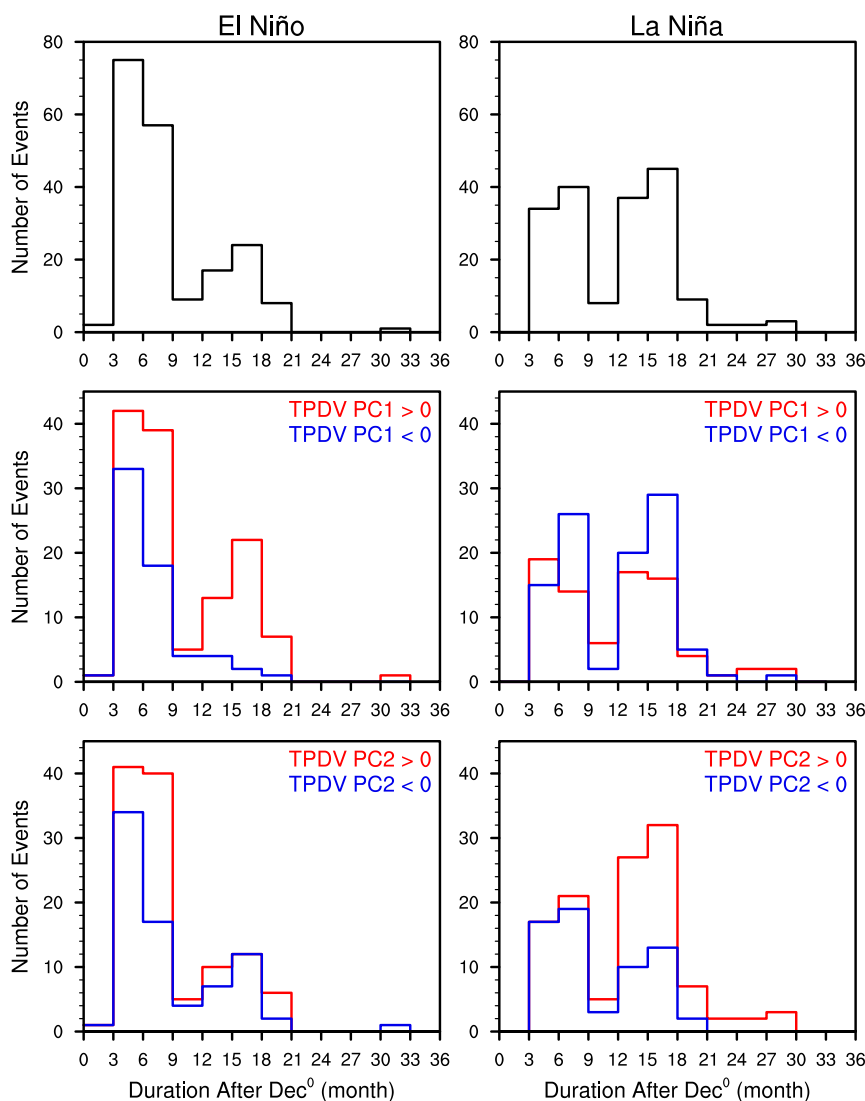


FIG. 5. Histograms of (left) El Niño and (right) La Niña duration for (top) the entire CCSM4 simulation and the positive (red) and negative (blue) phases of the (middle) first and (bottom) second TPDV modes. The duration of El Niño (La Niña) events is defined as the number of months for which the Niño-3.4 index remains above 0.25 (below -0.25) standard deviations after Dec⁰.

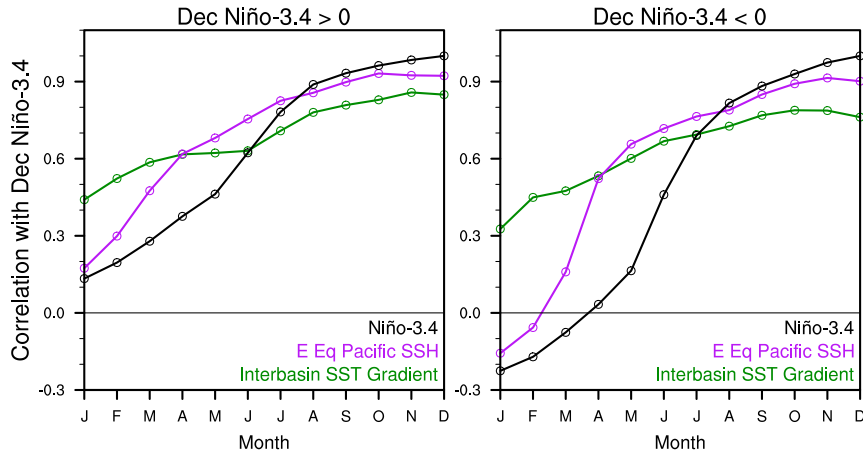


FIG. 6. Correlations of the December Niño-3.4 index with the Niño-3.4 index (black), SSH in the eastern equatorial Pacific (3°S – 3°N , 150° – 80°W ; purple), and interbasin SST gradient (10°S – 10°N , 140°E – 80°W minus 10°S – 10°N , 50°W – 100°E ; green) for months of the same year in the CCSM4 control simulation. The correlations are calculated separately for the (left) positive and (right) negative December Niño-3.4 indices. The correlation values exceeding 0.1 are statistically significant at the 99% confidence level for the approximate sample size of 650. The interbasin SST gradient index is defined after one-sided regressions on the December Niño-3.4 index of the previous year are removed from the SST field.

The frequency of both El Niño and La Niña events increases during the positive phase of the second TPDV mode compared to the negative phase, as anticipated from the larger ENSO amplitude (Fig. 4). The onset timing and initial evolution of El Niño are similar between the positive and negative phases of the second TPDV mode, but the difference begins to develop in boreal summer, the equatorial cold season. During the positive phase of the second TPDV mode, El Niño develops more rapidly from boreal summer to the end of year 0 compared to the negative phase. These stronger El Niño events are terminated more rapidly after Dec⁰, leading to stronger La Niña events in the following year. The change in the amplitude of La Niña between the positive and negative phases of the second TPDV mode is less than that for El Niño. The stronger La Niña events during the positive phase of the second TPDV mode, however, become more persistent compared to the negative phase. It is 3 times more likely for La Niña events to last longer than a year after Dec⁰ during the positive phase of the second TPDV mode compared to the negative phase (Fig. 5).

In the following subsections, we extend the analysis beyond the Niño-3.4 index and explore the possible mechanisms of ENSO modulation and its relation to TPDV. In particular, we investigate how decadal changes in the tropical Pacific background state associated with the two TPDV modes may influence the properties of El Niño and La Niña. The feedback

of ENSO modulation on TPDV is discussed in section 4b.

b. Mechanisms of ENSO modulation

1) FREQUENCY

Why do El Niño events become more frequent during the positive phase of IPO in the CCSM4 simulation? To answer this question, we first need to understand how El Niño and La Niña events are initiated. Figure 6 shows one-sided correlation coefficients of the December Niño-3.4 index with the Niño-3.4 index and SSH in the eastern equatorial Pacific (3°S – 3°N , 150° – 80°W) for the preceding months of the same year. (In this study, SSH is used as a proxy of the thermocline depth.) In CCSM4, Niño-3.4 SST anomalies associated with both El Niño and La Niña events develop from late boreal spring to mid-summer, with the correlations to the December Niño-3.4 index reaching 0.7–0.8 by July. The associated SSH anomalies develop a few months earlier, and the correlations to December Niño-3.4 index exceed 0.6 by May for both El Niño and La Niña. The most rapid growth of SSH anomalies occurs between February and April.

To examine what ocean–atmosphere state is related to the rapid development of SSH anomalies in the eastern equatorial Pacific that lead to El Niño and La Niña events in CCSM4, the positive and negative December Niño-3.4 indices are correlated with global SST and surface wind fields for February–April of the same year (Fig. 7, top).

Feb-Apr Surface Temperature/Wind Correlation with Dec Niño-3.4

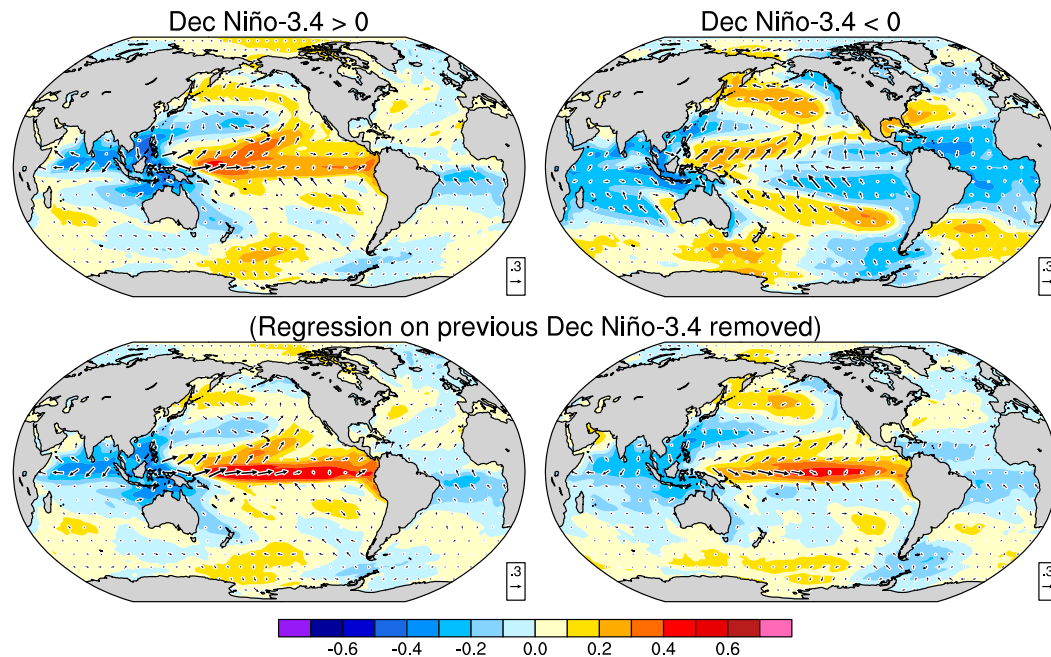


FIG. 7. (top) Correlation map of February–April global surface temperature (shading) and wind (vectors) anomalies with the December Niño-3.4 index of the same year in the CCSM4 control simulation. (bottom) As in (top), but one-sided regressions on the December Niño-3.4 index of the previous year are removed from the February–April surface temperature and wind fields prior to the correlation analysis. The correlations are calculated separately for the (left) positive and (right) negative December Niño-3.4 indices. The correlation values exceeding 0.1 are statistically significant at the 99% confidence level for the approximate sample size of 650.

Consistent with the analyses presented earlier, the correlation patterns are asymmetric between El Niño and La Niña, with La Niña being preceded more by the opposite phase of ENSO. The ENSO state prior to the El Niño and La Niña onset, however, varies greatly among individual events (cf. Fig. 4), resulting in weak SST correlations in the tropical Pacific ($r \approx 0.2$). To investigate what deviations from the average cycle of ENSO affect the development of ENSO events, the same one-sided correlation analysis is conducted after the effects of previous ENSO events are removed from the February–April SST and surface wind fields using one-sided regressions based on the previous year’s December Niño-3.4 index (Fig. 7, bottom). The resultant correlation patterns are overall symmetrical between El Niño and La Niña: tropical SST correlations are positive and larger in the Pacific and negative in the Indian and Atlantic Oceans, with positive zonal wind correlations in the western equatorial Pacific. These zonal wind anomalies would affect SSH in the eastern equatorial Pacific in the following season via excitation of equatorial Kelvin waves.

Although the causality of these SST and wind anomalies leading to ENSO events will require

further investigation, this result suggests that the SST gradient between the tropical Pacific and Atlantic or Indian Oceans is an important factor for the development of both El Niño and La Niña events. Indeed, the December Niño-3.4 index is significantly correlated with the interbasin SST gradient index (10°S – 10°N , 140°E – 80°W minus 10°S – 10°N , 50°W – 100°E ; the effect of previous ENSO events is removed as in Fig. 7) in February–April for both El Niño and La Niña, leading the correlations with SSH in the eastern equatorial Pacific (Fig. 6). The December Niño-3.4 index is more highly correlated with the interbasin SST gradient index than with the tropical Pacific SST index alone (10°S – 10°N , 140°E – 80°W) in February–April ($r = 0.74$ and 0.65 , respectively, based on two-sided correlation). Observational analysis shows a similar sensitivity of the El Niño and La Niña onset to interbasin SST gradient anomalies, although the relationship is not as robust as in CCSM4 (not shown). This result is also consistent with previous studies suggesting the impacts of SST variability outside the tropical Pacific on ENSO and TPDV (e.g., Latif and Barnett 1995; Wang 2006; Dong et al. 2006; Jansen et al. 2009; Okumura et al. 2011; Ding et al. 2012; Kang et al. 2014; McGregor et al. 2014;

Chikamoto et al. 2015). Given that ENSO exerts strong influences on SST variability in the Atlantic and Indian Oceans (e.g., Xie and Carton 2004; Schott et al. 2009), this result suggests two-way interactions between the tropical Pacific and Atlantic or Indian Oceans.

The deviations of interbasin SST gradients from the average ENSO cycle can be caused by multiple factors, including different decay timing of previous ENSO events, internal variability in the Atlantic and Indian Oceans, or changes in the background state of the tropical oceans. During the positive phase of IPO, all the tropical oceans become warmer, but the tropical Pacific warms more than the Atlantic and Indian Oceans (Fig. 3). This interdecadal shift in the background interbasin SST gradient may increase the chance of El Niño development during the positive phase of IPO. Figure 8 presents the relations of the February–April interbasin SST gradient, May–June SSH in the eastern equatorial Pacific, and December Niño-3.4 index for the positive and negative phases of IPO. As in Figs. 6 and 7, the effect of previous ENSO events is removed from the interbasin SST gradient index using the regression analysis based on the previous year’s December Niño-3.4 index. The February–April interbasin SST gradient index is highly correlated with both May–June equatorial Pacific SSH ($r = 0.79$) and December Niño-3.4 index ($r = 0.74$) for the entire 1300-yr simulation. Figure 8 shows that the increased occurrence of El Niño during the positive phase of IPO is indeed related to the positive bias in the interbasin SST gradient index compared to the negative phase. The difference between the positive and negative phases of IPO is not very clear for La Niña in Fig. 8, but the occurrence of La Niña events that develop from neutral condition does increase in association with the negative bias in the interbasin SST gradient index during the negative phase of IPO (not shown).

2) DURATION

El Niño events tend to terminate quickly after the mature phase, while La Niña events often persist for another year (Fig. 2). Not every event follows this composite evolution, and the duration of El Niño and La Niña varies greatly from event to event (Figs. 4 and 5). As shown earlier, most El Niño events that last longer than a year after Dec⁰ occur during the positive phase of IPO in CCSM4. Three-fourths of multiyear La Niña events, on the other hand, occur during the positive phase of the second TPDV mode, the period of strong ENSO. What are the factors that affect the evolution of El Niño and La Niña after the first peak in Dec⁰ and hence their duration? Figures 9 and 10 show the composite evolution of equatorial SST, surface wind, precipitation, and SSH anomalies for El Niño and La Niña events for which the sign of Niño-3.4 index

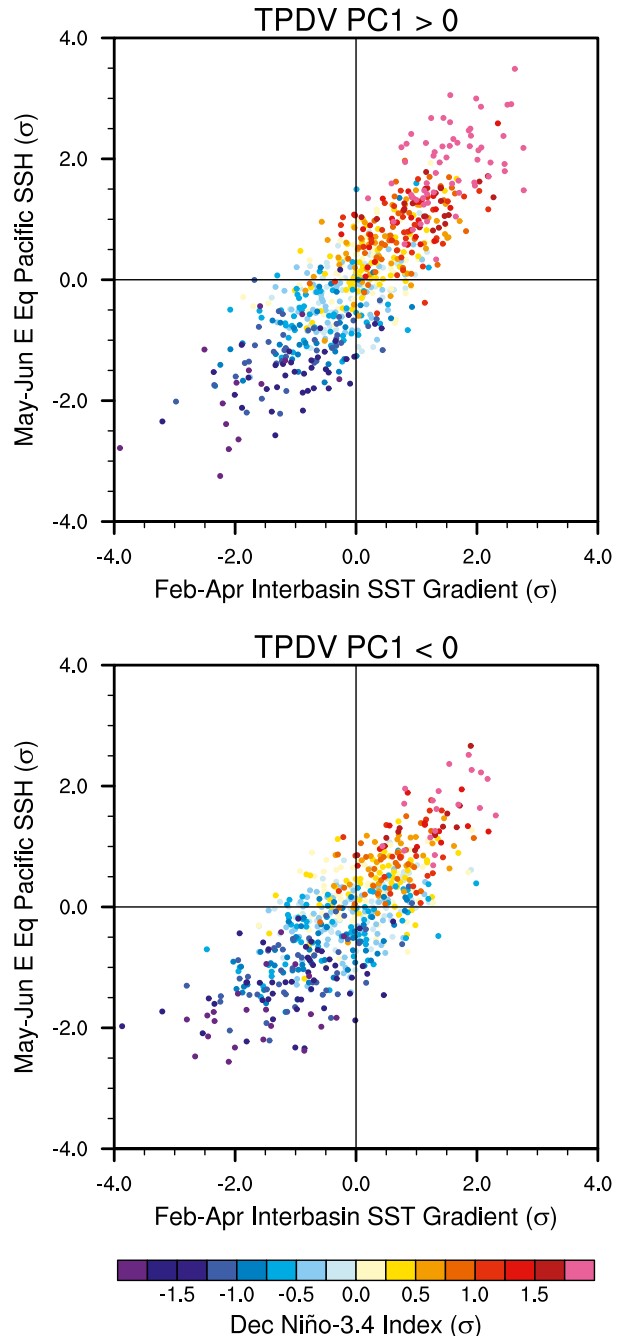


FIG. 8. Scatterplots of the February–April interbasin SST gradient (10°S – 10°N , 140°E – 80°W minus 10°S – 10°N , 50°W – 100°E) vs the May–June SSH in the eastern equatorial Pacific (3°S – 3°N , 150° – 80°W) for the (top) positive and (bottom) negative phases of the first TPDV mode in the CCSM4 control simulation. The color of each dot indicates the value of the same year’s December Niño-3.4 index. The interbasin SST gradient index is defined after one-sided regressions on the December Niño-3.4 index of the previous year are removed from the SST field. All the indices are shown in standard deviation units. The interbasin SST gradient index is correlated with the SSH (Niño-3.4) index at $r = 0.79$ (0.74) for the entire 1300-yr simulation.

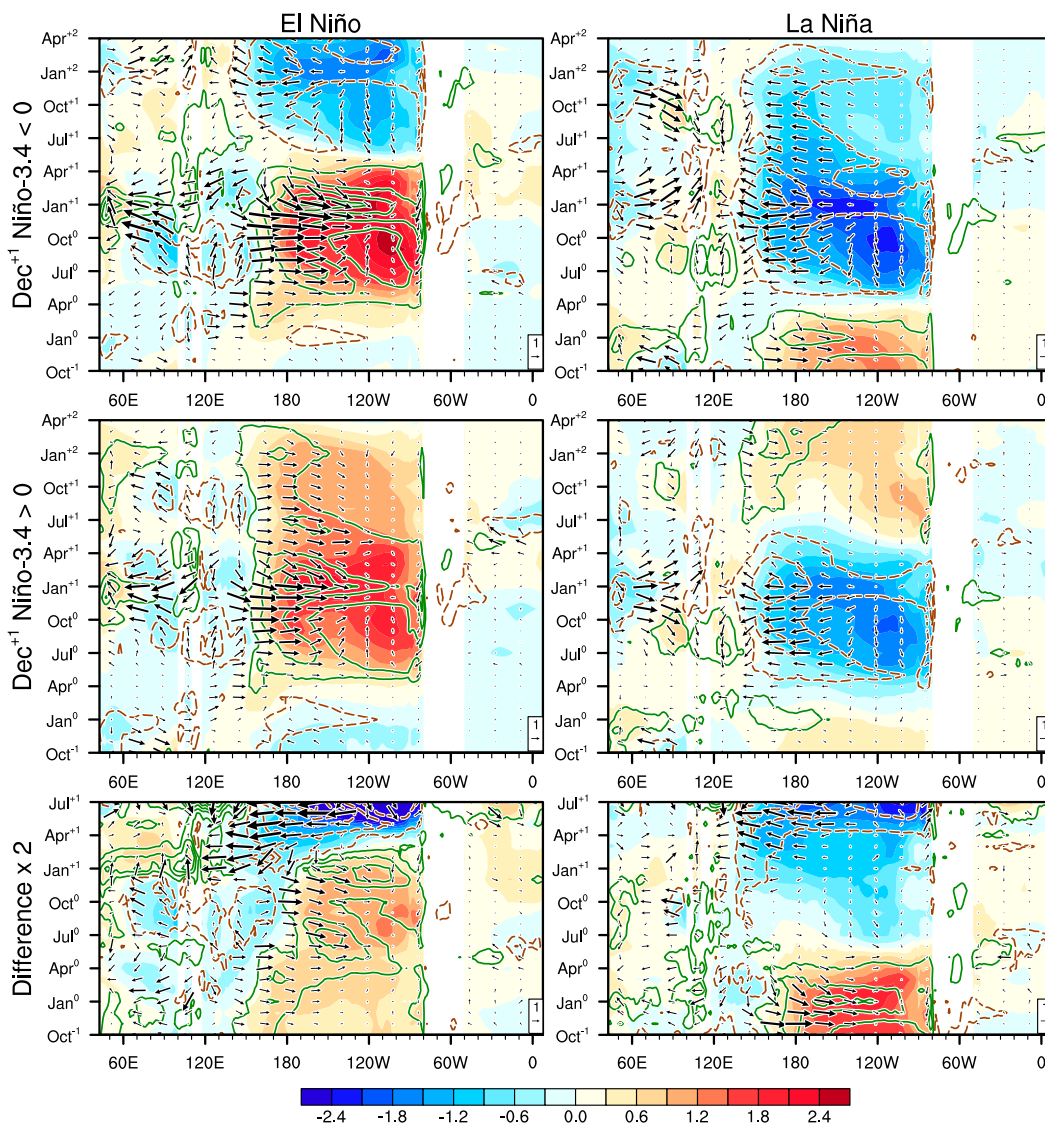


FIG. 9. Longitude–time cross sections of composite SST ($^{\circ}\text{C}$; shading), surface wind (m s^{-1} ; vectors), and precipitation [positive (negative) contours in green solid (brown dashed) at $\pm 1, 3, 5, \dots$ mm day^{-1}] anomalies along the equator (3°S – 3°N) for Oct^{-1} – Apr^{+2} of (left) El Niño and (right) La Niña events with (top) negative and (middle) positive Dec^{+1} Niño-3.4 index in the CCSM4 control simulation. (bottom) Difference between (top) and (middle) multiplied by 2 for Oct^{-1} – Jul^{+1} .

changes or remains the same in Dec^{+1} . These figures suggest that one of the important factors for the duration of El Niño and La Niña is the amplitude of events: stronger El Niño events terminate more quickly, while stronger La Niña events last longer compared to weaker events. These stronger and longer La Niña events are preceded by stronger El Niño events and the associated larger upwelling Kelvin waves propagating from the western equatorial Pacific, compared to weaker and shorter La Niña events. As discussed in previous studies, this asymmetry in the duration of strong El Niño and La Niña events arises

from nonlinearity in the tropical ocean–atmosphere system. For example, asymmetric response of tropical Pacific precipitation to El Niño and La Niña makes surface winds more susceptible to negative feedback from the Indian Ocean during El Niño than La Niña (e.g., Okumura et al. 2011; Ohba and Watanabe 2012), while the nonlinearity in the thermocline feedback slows down the termination of La Niña events compared to El Niño (e.g., Meinen and McPhaden 2000; DiNezio and Deser 2014).

In addition to the amplitude, there is another important factor that appears to affect the duration of ENSO

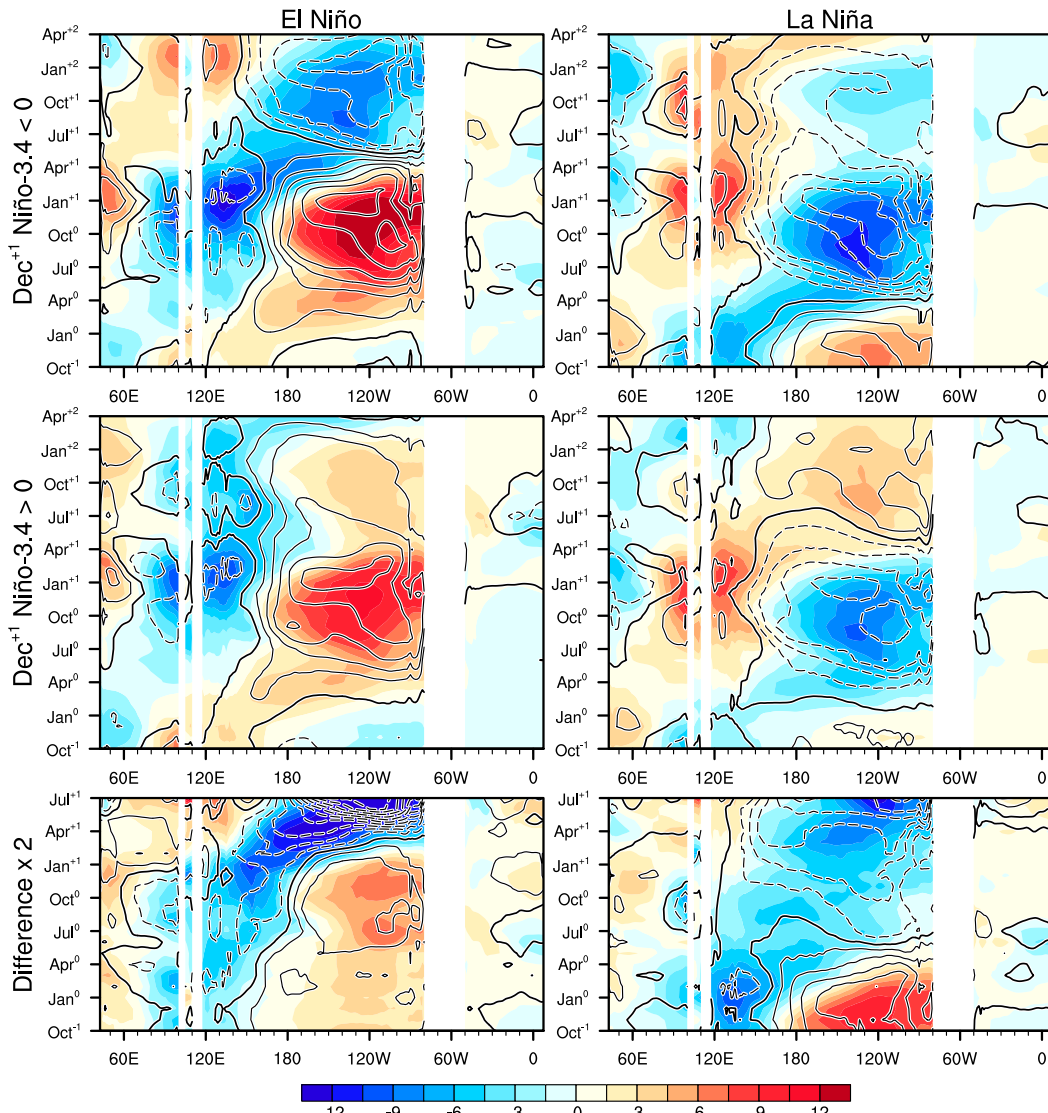


FIG. 10. As in Fig. 9, but for composite SSH (cm; shading) and SST (black contours at intervals of 0.4°C ; zero contours thickened) anomalies.

events (Figs. 9 and 10). El Niño and La Niña events that terminate after the mature phase tend to develop earlier during year 0 compared to multiyear events. The earlier onset of ENSO events leads to earlier development of SSH anomalies in the eastern equatorial Indian Ocean and stronger response of the Indian Ocean dipole mode in boreal fall compared to multiyear events. During multiyear ENSO events, SSH anomalies of similar magnitude develop over the eastern equatorial Indian Ocean in boreal winter but do not strongly affect SSTs as the seasonal upwelling subsides after fall. Basinwide SST anomalies over the Indian Ocean, which develop after the dipole response decays and have the same sign as Pacific SST anomalies,

are slightly stronger during single-year than multiyear ENSO events. SST anomalies of the same sign also develop earlier in the tropical Atlantic during single-year than multiyear ENSO events. Thus, the timing of ENSO event onset and attendant development of SST anomalies in the other tropical oceans appear to be another factor affecting the duration of El Niño and La Niña events. This factor can also be understood in terms of the interbasin SST gradient: the early adjustment of the Atlantic and Indian Oceans to Pacific SST anomalies weakens the interbasin SST gradient anomalies and may hasten the termination of ENSO events.

Figure 11 shows the relation between the duration of El Niño and La Niña events and the first factor, their

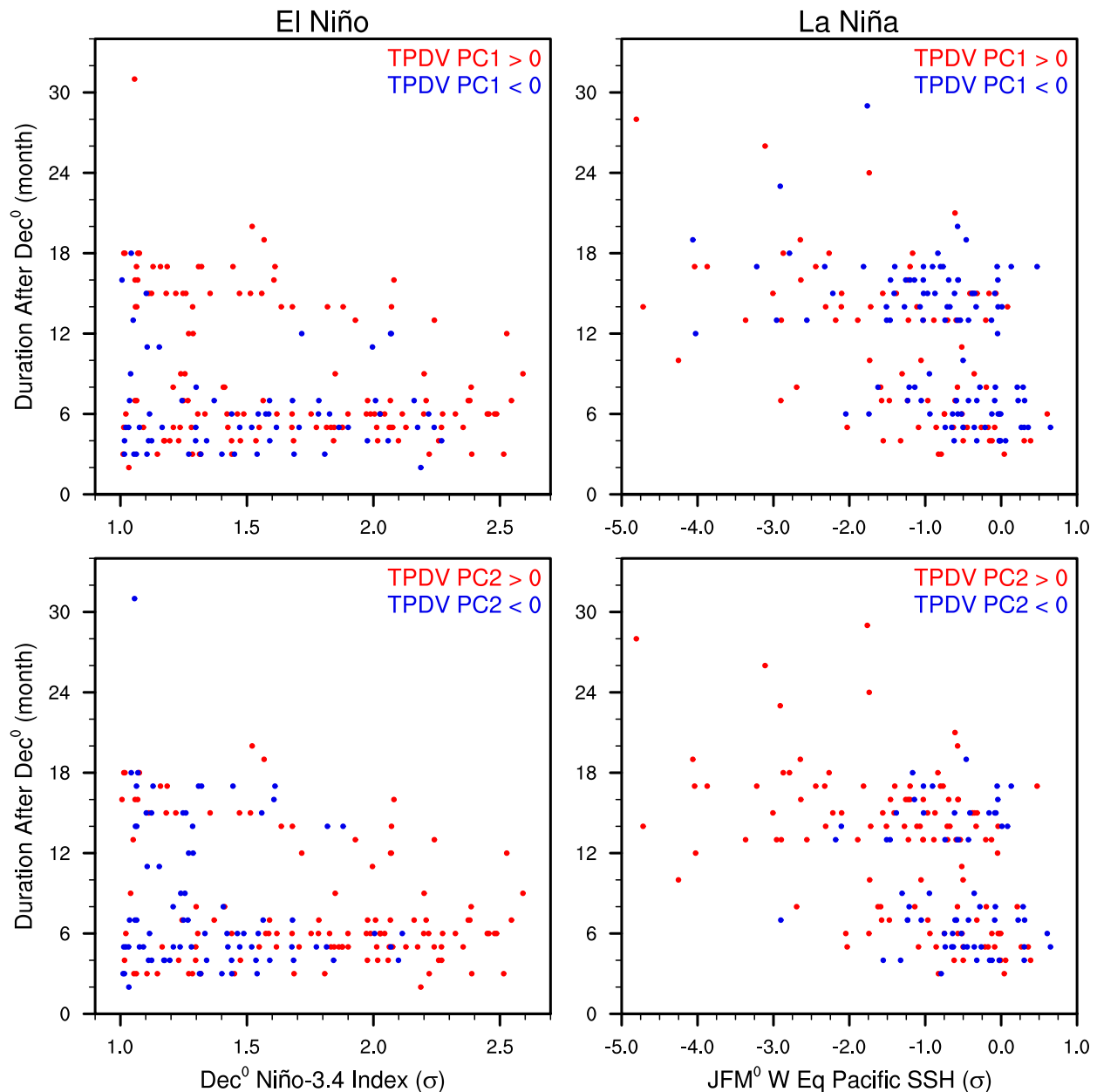


FIG. 11. Scatterplots of (left) the Dec⁰ Niño-3.4 index vs the duration of El Niño events and (right) the Jan⁰–Mar⁰ (JFM⁰) SSH in the western equatorial Pacific (3°S–3°N, 140°E–160°W) vs the duration of La Niña events in the CCSM4 control simulation. (top) ENSO events that occur during the positive and negative phases of the first TPDV mode are shown by red and blue dots, respectively. (bottom) As in (top), but for the second TPDV mode. The duration of El Niño (La Niña) events is defined as the number of months for which the Niño-3.4 index remains above 0.25 (below -0.25) standard deviations after Dec⁰.

amplitude, for the positive and negative phases of the two TPDV modes. For simplicity, we use the Dec⁰ Niño-3.4 index for the index of El Niño amplitude. For the index of La Niña amplitude, we instead use Jan⁰–Mar⁰ SSH in the western equatorial Pacific (3°S–3°N, 140°E–160°W) because this is one of the most prominent precursors of La Niña duration (Fig. 10) and is linked to the amplitude of La Niña that follows, as will be discussed in the

next section. Figure 11 confirms that the amplitude is indeed an important factor for the duration of both El Niño and La Niña events. The majority of strong El Niño events for which the Dec⁰ Niño-3.4 index exceeds 1.75 standard deviation terminate within 7 months after Dec⁰ [58 out of 72 events (81%)], and these strong and short El Niño events occurs mostly during the positive phase of the second TPDV mode [51 out of 58 events

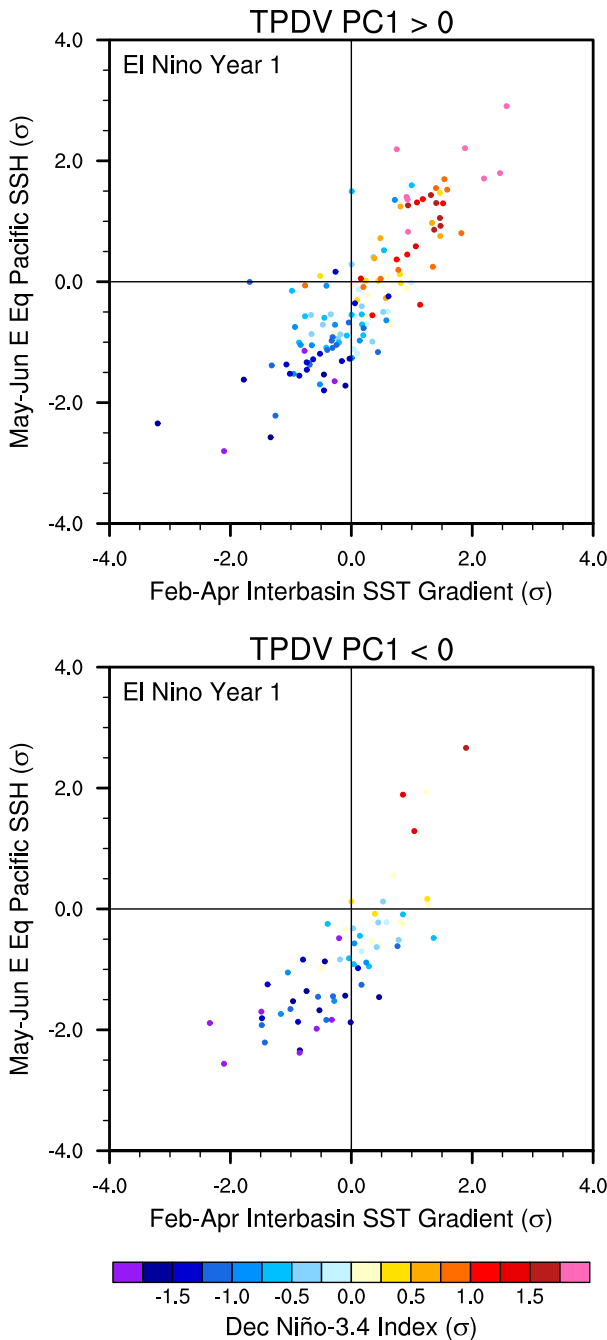


FIG. 12. As in Fig. 8, but only for year 1 of El Niño events.

(88%); Fig. 11, bottom left). The weaker El Niño events exhibit bimodal distribution of their duration and the majority of the weaker events that last longer than 7 months occur during the positive phase of IPO [41 out of 50 events (82%); Fig. 11, top left]. Most La Niña events preceded by large negative SSH anomalies over the western equatorial Pacific in Jan⁰–Mar⁰ (less than -1.75 standard deviation), on the other hand, last longer than a year after Dec⁰ [31 out of 36 events

(86%)], and these strong and long La Niña events happen mostly during the positive phase of the second TPDV mode [29 out of 31 events (94%); Fig. 12, bottom right]. The weaker La Niña events show bimodal distribution of their duration, but there is no clear bias in the distribution between the positive and negative phases of both the TPDV modes.

The second factor appears to play an important role for the increased occurrence of multiyear El Niño events during the positive phase of IPO. There is no significant change in the timing and amplitude of SST anomalies outside the tropical Pacific between the positive and negative phases of IPO (not shown). However, El Niño-like changes in the background state increase the interbasin SST gradient toward the tropical Pacific during the positive phase of IPO compared to the negative phase (Fig. 3). The frequent occurrence of multiyear El Niño events during the positive phase of IPO is indeed associated with the positive bias in the interbasin SST gradient in Feb⁺¹–Apr⁺¹ (Fig. 12). During the negative phase of IPO, the same mechanism acts to increase the duration of La Niña events compared to the negative phase, but this effect is nearly counteracted by the decrease in the number of La Niña following El Niño, which tends to be stronger and last longer than La Niña that develops from neutral condition (not shown). The relative role of these different factors for the ENSO event duration will need to be studied further in both models and observations.

3) AMPLITUDE AND PATTERN

In CCSM4, both El Niño and La Niña become stronger during the positive phase of the second TPDV mode, consistent with previous modeling studies. El Niño and La Niña, however, intensify for different reasons. Figures 13 and 14 present the composite evolution of equatorial Pacific SST, surface wind, precipitation, and SSH anomalies for El Niño and La Niña events that occur during the positive and negative phases of the second TPDV mode. The main difference between the positive and negative phases of the second TPDV mode is found for El Niño from late boreal spring to winter, the season when the equatorial Pacific cold tongue develops and the Bjerknes feedback strengthens. During the positive phase of the second TPDV mode, positive precipitation anomalies associated with equatorial warming become enhanced and displaced eastward compared to the negative phase. The related increase in westerly wind anomalies over the central Pacific deepens the thermocline and enhances positive SST anomalies in the eastern Pacific, resulting in rapid development of El Niño (cf. Fig. 4). During the positive

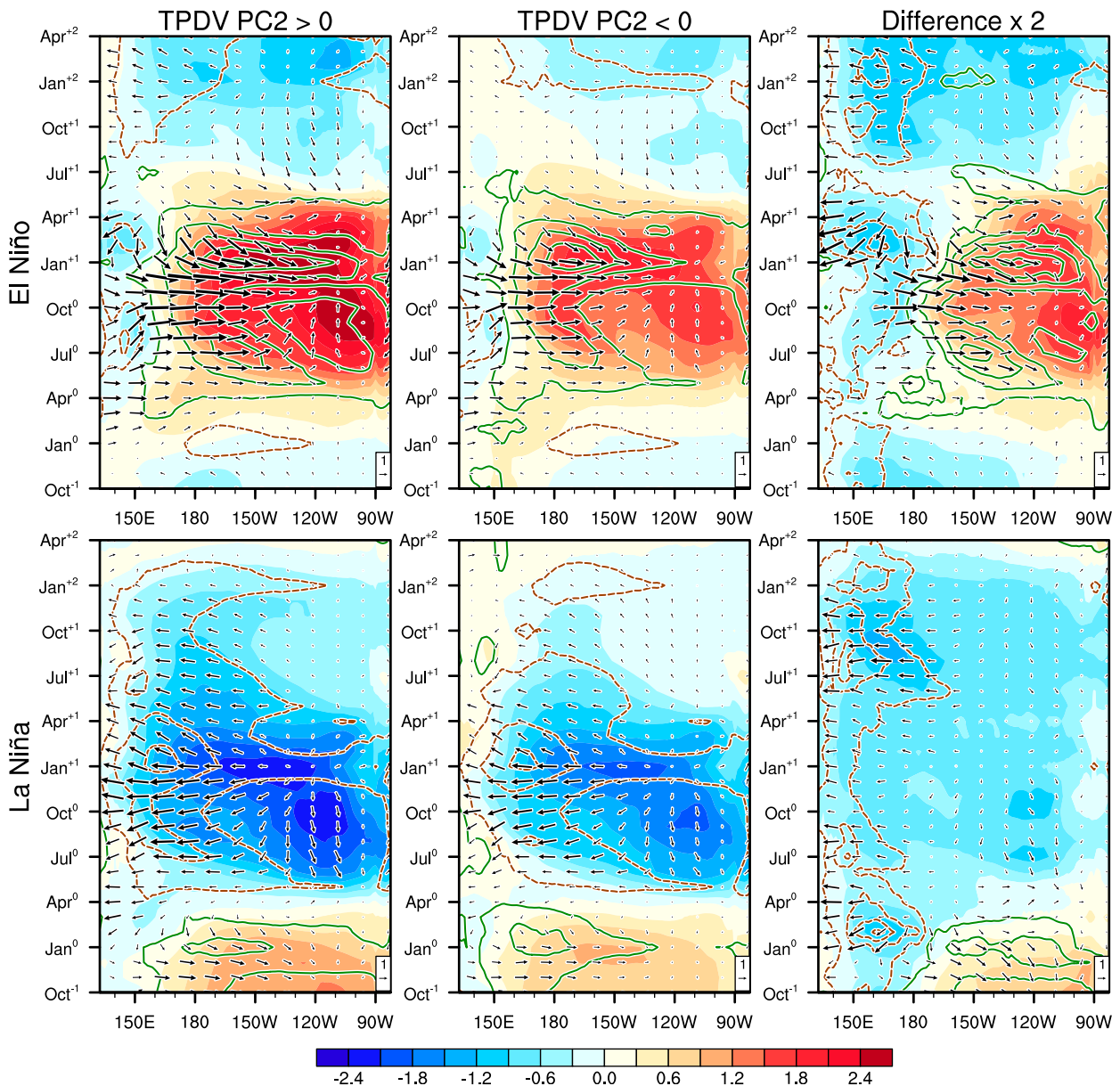


FIG. 13. Longitude–time cross sections of composite SST ($^{\circ}\text{C}$; shading), surface wind (m s^{-1} ; vectors), and precipitation [positive (negative) contours in green solid (brown dashed) at $\pm 1, 3, 5, \dots \text{mm day}^{-1}$] anomalies along the equator (3°S – 3°N) for Oct^{-1} – Apr^{+2} of (top) El Niño and (bottom) La Niña events that occur during the (left) positive and (center) negative phases of the second TPDV mode in the CCSM4 control simulation. (right) Difference between (left) and (center) multiplied by 2.

phase of the second TPDV mode, this eastward shift of ocean–atmosphere anomalies could lead to the development of anomalous easterly winds in the far western Pacific after the mature phase of El Niño, which would force an upwelling Kelvin wave and initiate La Niña in year 1.

The intensification of La Niña during the positive phase of the second TPDV mode, on the other hand, is caused by the intensification of the preceding El Niño and attendant upwelling Kelvin wave (Figs. 13 and 14).

The difference in the amplitude of the preceding El Niño, however, is not statistically significant in Fig. 4. During the positive phase of the second TPDV mode, there are increased occurrences of a La Niña event that follows a strong El Niño but takes two years to fully develop, similar to the observed La Niña events in 1983–86 and 1998–2001. The effect of El Niño amplitude on the following La Niña’s amplitude becomes more evident when these slow-developing La Niña events are separated in the composite analysis (not shown).

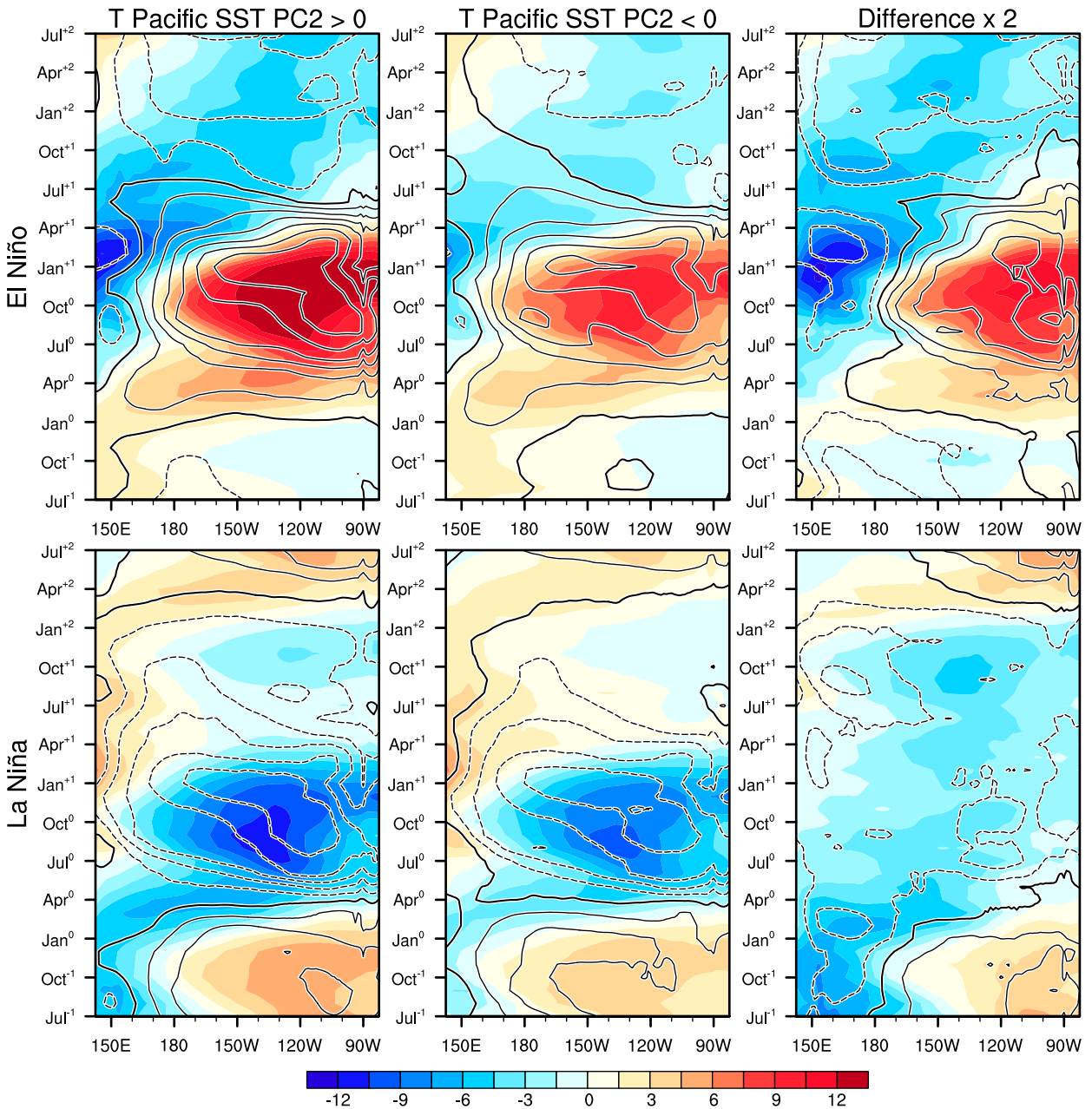


FIG. 14. As in Fig. 13, but for composite SSH (cm; shading) and SST (black contours at intervals of 0.4°C; zero contours thickened) anomalies.

Figures 13 and 14 also show that stronger equatorial cooling during the positive phase of the second TPDV mode increases negative precipitation and easterly surface wind anomalies over the western Pacific compared to the negative phase, which may contribute to the longer duration of La Niña events.

The spatial patterns of ocean–atmosphere anomalies also show asymmetric changes between El Niño and La Niña in association with the second TPDV mode. One-sided regression analysis is conducted

based on the Niño-3.4 index for all months that fall on the positive and negative phases of the second TPDV mode in Fig. 15. For the positive unit Niño-3.4 index, tropical Pacific SST and precipitation anomalies become larger in the east and smaller in the west during the positive than the negative phase of TPDV, with stronger westerly wind anomalies in the central Pacific. Positive precipitation anomalies in the eastern Pacific are centered closer to the equator during the positive than the negative phase of TPDV. These changes in the

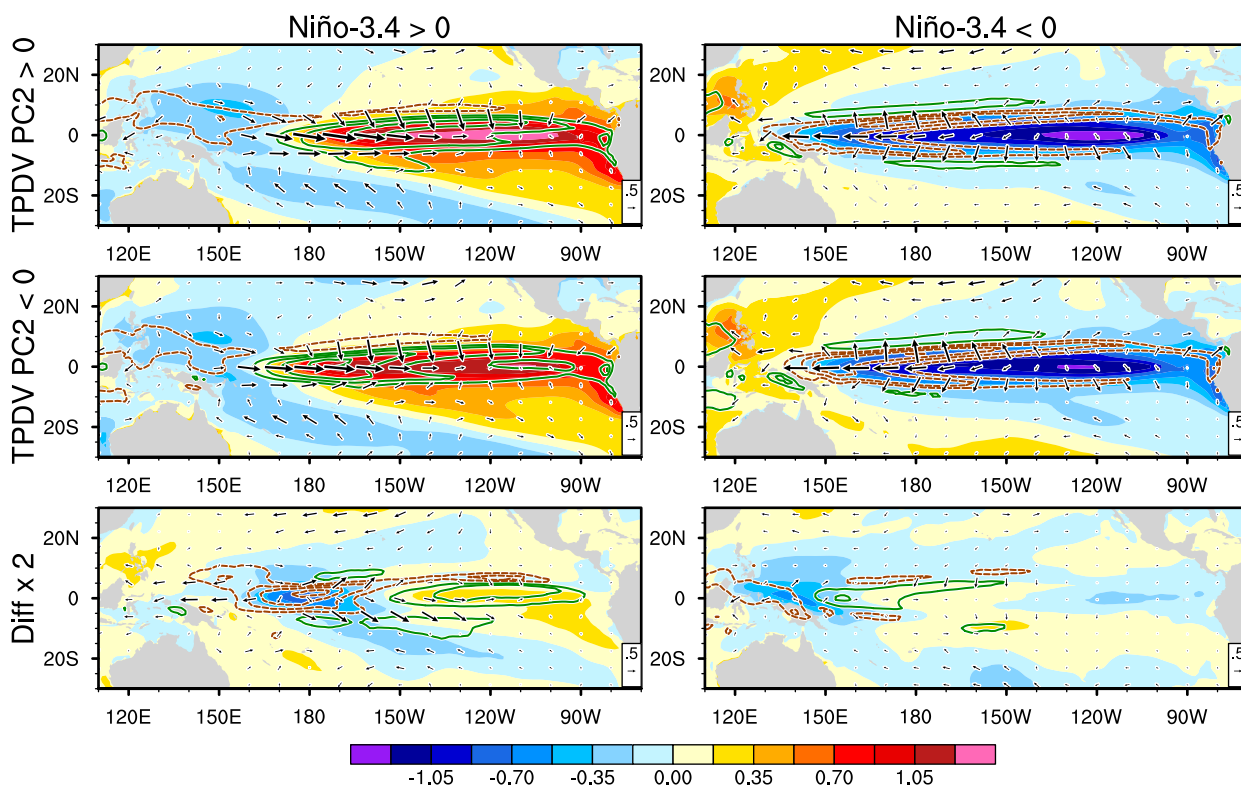


FIG. 15. One-sided regression maps of tropical Pacific SST ($^{\circ}\text{C}$; shading), surface wind (m s^{-1} ; vectors), and precipitation [positive (negative) contours in green solid (brown dashed) at intervals of 1 mm day^{-1}] anomalies on the (left) positive and (right) negative Niño-3.4 index during the (top) positive and (middle) negative phases of the second TPDV mode in the CCSM4 control simulation. (bottom) Difference between (top) and (middle) multiplied by 2. The sign of regression on the negative Niño-3.4 index is reversed. The regression coefficients are for 1°C of the Niño-3.4 index. The regression analysis is not stratified by season, and all months that fall on the positive and negative phases of the second TPDV mode are used.

El Niño anomaly pattern are seen throughout the year but most prominent in boreal summer, when El Niño starts to develop (not shown). It should also be noted that these changes in the El Niño anomaly pattern are much like the decadal changes in the background state associated with the second TPDV mode (cf. Fig. 3). For La Niña, one-sided regression analysis based on the negative Niño-3.4 index suggests that negative equatorial SST anomalies extend farther to the west during the positive phase of the second TPDV mode compared to the negative phase, but there is no other significant change in the anomaly pattern over the central and eastern Pacific. Ogata et al. (2013) suggest that nonlinearity in the zonal temperature advection causes this westward extension of La Niña SST anomalies during the period of strong ENSO. This differing modulation of ENSO patterns results in stronger asymmetry in the pattern of El Niño and La Niña during the positive phase of the second TPDV mode compared to the negative phase.

Why do the spatial pattern and seasonal evolution of ocean-atmosphere anomalies modulate mainly for El Niño in association with the second TPDV mode? To

investigate the role of nonlinearity in atmospheric processes for the asymmetric ENSO modulation, we conduct standalone CAM4 experiments by prescribing monthly SSTs for composite El Niño and La Niña events with changes in the background SSTs associated with the second TPDV mode (see section 2d for methods). Figure 16 compares the seasonal evolution of ensemble-mean equatorial precipitation and surface wind response in these CAM4 experiments along with SST forcing. In CAM4, the cooler background SST in the western tropical Pacific enhances negative precipitation anomalies for both El Niño and La Niña. The warmer background SST in the eastern tropical Pacific, on the other hand, increases equatorial precipitation response only for El Niño, in agreement with the analysis of CCSM4 simulation. The difference in the atmospheric response to El Niño between the positive and negative phases of TPDV is much smaller in CAM4 than in CCSM4, but these small changes would likely be amplified through the Bjerknes feedback when the CAM4 is coupled to the ocean.

The asymmetric changes in the atmospheric response to El Niño and La Niña in CAM4 can be explained by the

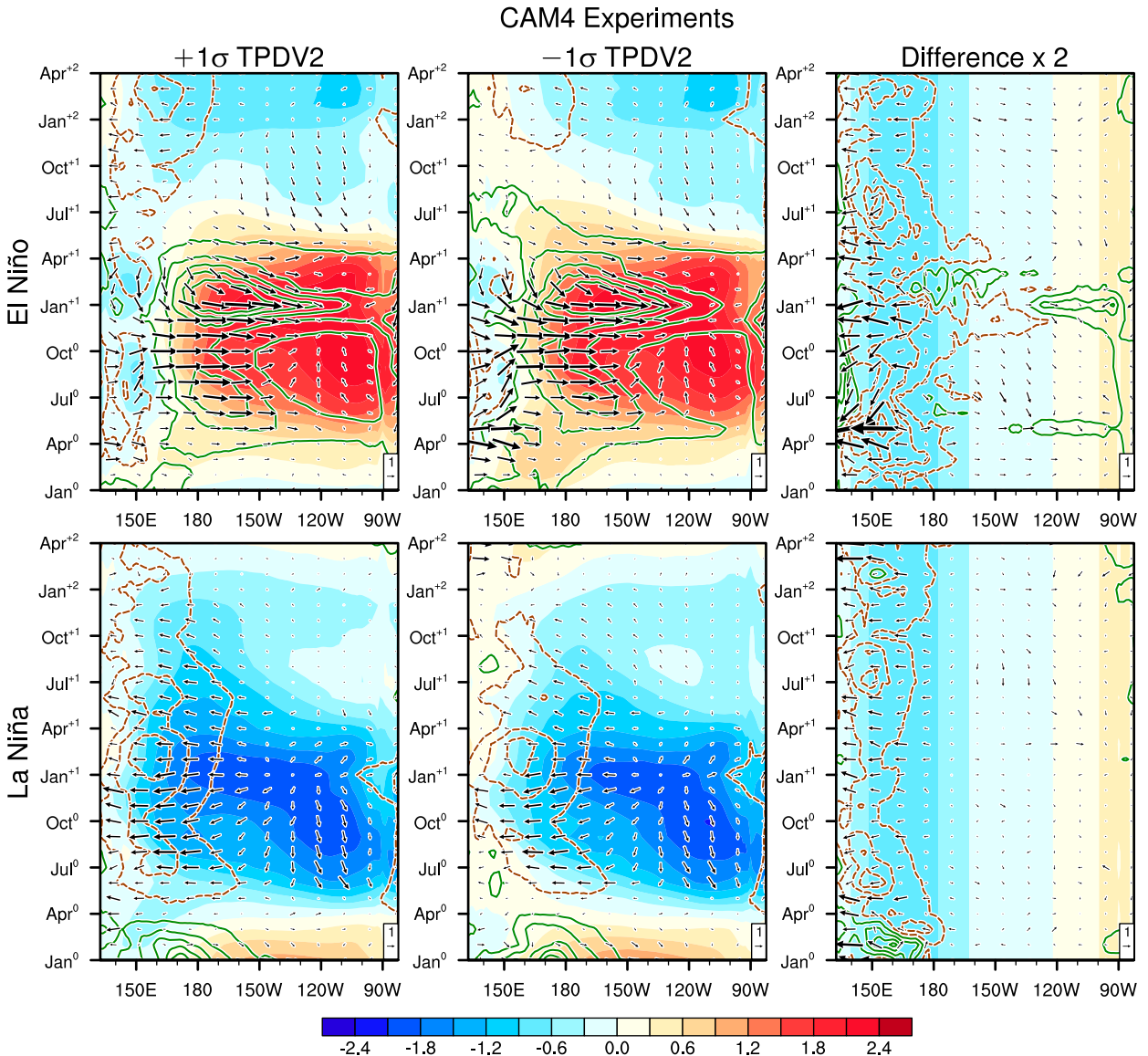


FIG. 16. Longitude–time cross sections of the ensemble-mean equatorial Pacific (3°S–3°N) surface wind (m s^{-1} ; vectors) and precipitation [positive (negative) contours in green solid (brown dashed) at $\pm 1, 3, 5, \dots \text{mm day}^{-1}$] response for Jan^0 – Apr^{+2} in the standalone CAM4 experiments forced with the composite (top) El Niño and (bottom) La Niña SST anomalies ($^{\circ}\text{C}$; shading) and the background SST changes for the (left) positive and (center) negative phases of the second TPDV mode based on the CCSM4 control simulation. (right) Difference between (left) and (center) multiplied by 2.

nonlinear relation between the atmospheric deep convection and SSTs over the eastern equatorial Pacific (Fig. 17). In this region, the sharp gradient of background SSTs due to the presence of the equatorial cold tongue causes the atmospheric convergence and resultant deep convection over the warmest SSTs just north of the equator. Climatological precipitation rates during the equatorial cold season increase exponentially, with SSTs over 26°C in this region. The warming associated with El Niño can elevate equatorial SSTs above this convective threshold, and an increase in the

background SSTs facilitates this change. The cooling associated with La Niña, on the other hand, does not significantly affect the already cold and dry condition in the equatorial Pacific, and decadal changes in the background SSTs are too small to modulate this precipitation response to La Niña. Takahashi and Dewitte (2016) suggest that this convective SST threshold causes nonlinear regimes of strong and moderate El Niño.

The background SST changes associated with IPO have similar asymmetric influence on the anomaly patterns of El Niño and La Niña, but their impact is much

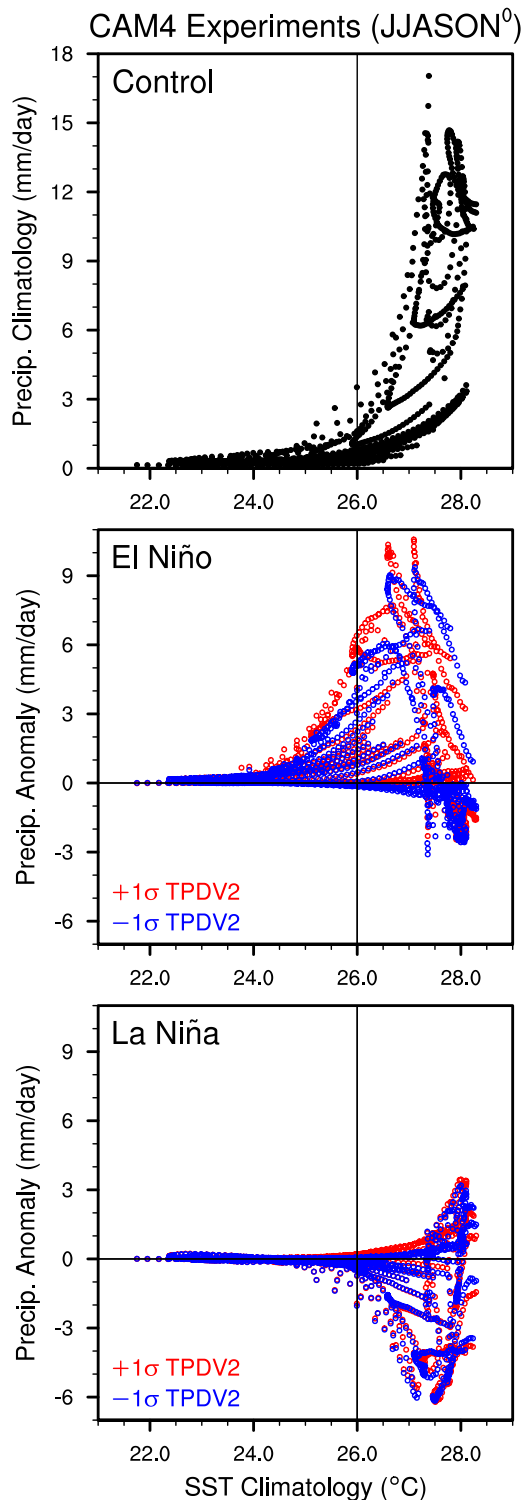


FIG. 17. Scatterplots of June–November SST climatology vs (top) June–November precipitation climatology in the CAM4 control simulation and Jun⁰–Nov⁰ ensemble-mean precipitation response in the CAM4 (middle) El Niño and (bottom) La Niña experiments over the eastern tropical Pacific (10°S–10°N, 150°–80°W). In (middle), (bottom), red and blue circles show the El Niño/La Niña experiments with the background SST changes associated with the positive and negative phases of the second TPDV mode, respectively.

weaker compared to the second TPDV mode (not shown). In addition to the magnitude of background SST changes, their spatial pattern and influence on the SST gradient may also play an important role. Note that the second TPDV mode affects both the zonal and meridional gradients of background SSTs while the IPO has minimal impact on the zonal SST gradient (Fig. 3). In support of these findings, recent studies of anthropogenic ENSO changes show that the spatial pattern of tropical Pacific SST warming has a similar nonlinear impact on the precipitation response to El Niño and La Niña (Cai et al. 2014; Chung et al. 2014; Chung and Power 2014; Zheng et al. 2016).

4. Discussions

a. Origins of TPDV

What causes the decadal changes in the background state associated with ENSO modulation? Some previous studies argue that TPDV may be generated by decadal changes in ENSO, rather than the other way around (e.g., Rodgers et al. 2004; Vimont 2005). The patterns of TPDV in CCSM4, however, have resemblance to those in the CAM4-SOM control simulation, in which the Bjerknes feedback, a mechanism crucial for the interannual variability of ENSO, is absent (cf. Figs. 3 and 18). In agreement with the multimodel study by Clement et al. (2011), the IPO simulated in CCSM4 is similar to the leading mode of TPDV in CAM4-SOM, albeit with weaker anomalies over the equatorial and North Pacific in CAM4-SOM compared to CCSM4. The power spectra of the Niño-3.4 index are not significantly different between CCSM4 and CAM4-SOM on decadal and longer time scales (Okumura 2013), although the relative importance of ocean dynamics may be model dependent (Clement et al. 2011). In CAM4-SOM, the ocean and atmosphere are coupled only through local surface heat fluxes, and therefore internal variability of the extratropical atmospheric circulation plays an important role in determining the large-scale patterns of SST variability. The stochastic atmospheric forcing is integrated by the ocean mixed layer and produces low-frequency SST variability in the extratropics (Frankignoul and Hasselmann 1977), which further influences the tropics through atmospheric teleconnections (Barnett et al. 1999; Pierce et al. 2000; Dommenget and Latif 2008). Recent studies suggest that the tropical Pacific is more strongly influenced by stochastic atmospheric forcing from the South Pacific than from the North Pacific because of the northward displacement of the ITCZ (Okumura 2013; Zhang

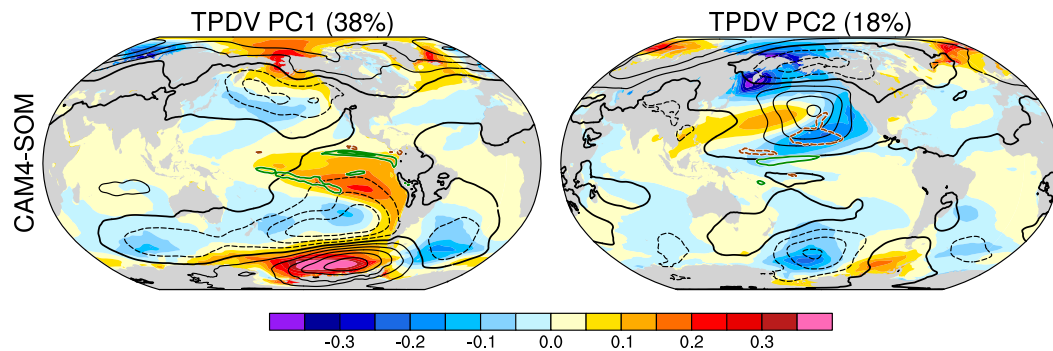


FIG. 18. Regression maps of global SST ($^{\circ}\text{C}$; shading), SLP (black contours at intervals of 0.1 hPa; zero contours thickened), and precipitation [positive (negative) contours in green solid (brown dashed) at intervals of 0.2 mm day^{-1}] anomalies on the (left) PC1 and (right) PC2 of TPDV in the CAM4-SOM control simulation. The PCs are standardized and SST, SLP, and precipitation data are smoothed with a 10-yr low-pass filter prior to the regression analysis. The first and second modes of TPDV explain 38% and 18% of the total low-pass-filtered variance, respectively.

et al. 2014b). In particular, the IPO simulated in CAM4-SOM is linked to the leading mode of atmospheric variability over the South Pacific, the PSA mode, which affects the strength of southeasterly trade winds over the southeast tropical Pacific. The attendant thermodynamic air–sea interactions within the tropical Pacific generate ENSO-like anomaly pattern (Dommenget 2010; Clement et al. 2011). This IPO driven by stochastic atmospheric variability may influence the frequency and duration of El Niño events in CCSM4 as discussed in the previous section. Although some studies suggest that stochastic atmospheric forcing also affects the development of interannual ENSO events (e.g., Vimont et al. 2001; Anderson 2003; Chang et al. 2007; Alexander et al. 2010; Zhang et al. 2014a), the modes of extratropical atmospheric variability (e.g., the NPO and PSA) are not directly linked to the decadal modulation of ENSO in the CCSM4 control simulation.

The global anomaly pattern associated with the second TPDV mode also has some resemblance between the CCSM4 and CAM4-SOM control simulations (Figs. 3 and 18). Although the zonal dipole pattern in the tropical Pacific is considerably weaker in CAM4-SOM compared to CCSM4, the extratropical ocean–atmosphere anomaly patterns are surprisingly similar between the two models over both the North and South Pacific. As in CCSM4, the extratropical SLP anomalies in CAM4-SOM project onto the NPO and PSA2 patterns. Both the NPO and PSA2 patterns arise from internal atmospheric dynamics and appear as the second leading EOF mode of monthly SLP variability over the extratropical North and South Pacific, respectively, in the CAM4 control simulations, as well as in CCSM4 and CAM4-SOM. To investigate the role of stochastic variability of these modes in generating the second leading mode of TPDV, the NPO and PSA2 PCs in CAM4-SOM and CCSM4 are

correlated with global SST and SLP in Fig. 19. In CAM4-SOM, the NPO and PSA2 modes are not significantly correlated with underlying SSTs on month-to-month time scales, confirming that they arise in the absence of SST forcing, but the correlations to tropical SSTs increase to 0.3–0.5 on decadal time scales. Intriguingly, the PSA2 mode is associated with a zonal dipole pattern of SSTs in the tropical Pacific, while the SST correlations with the NPO mode is limited mostly to north of the equator. The CCSM4 shows very similar correlation patterns with the NPO and PSA2 modes on decadal time scales. Compared to CAM4-SOM, the PSA2 mode in CCSM4 is more strongly correlated with the zonal dipole pattern of SSTs over the tropical Pacific and the correlations with North Pacific SLP extend farther to the north, projecting onto the NPO pattern. This result suggests that stochastic atmospheric variability over the South Pacific plays an important role also for the second leading mode of TPDV, which is associated with the decadal modulation of ENSO amplitude, as well as the asymmetry in the duration and pattern of El Niño and La Niña in CCSM4. The enhanced decadal SST anomalies over the tropical Pacific in CCSM4 may further affect the extratropical atmospheric circulation and SSTs over the North Pacific, inducing a basinwide decadal anomaly pattern.

b. Effect of ENSO modulation on TPDV

The equatorial ocean–atmosphere anomalies associated with the two TPDV modes are more pronounced in CCSM4 than in CAM4-SOM (cf. Figs. 3 and 18), suggesting the role of equatorial ocean dynamics in CCSM4. It is plausible that the ENSO modulation induced by stochastically forced changes in the background state, in turn, affects both the TPDV modes in CCSM4. During the positive phase of IPO, the increased occurrence and duration of El

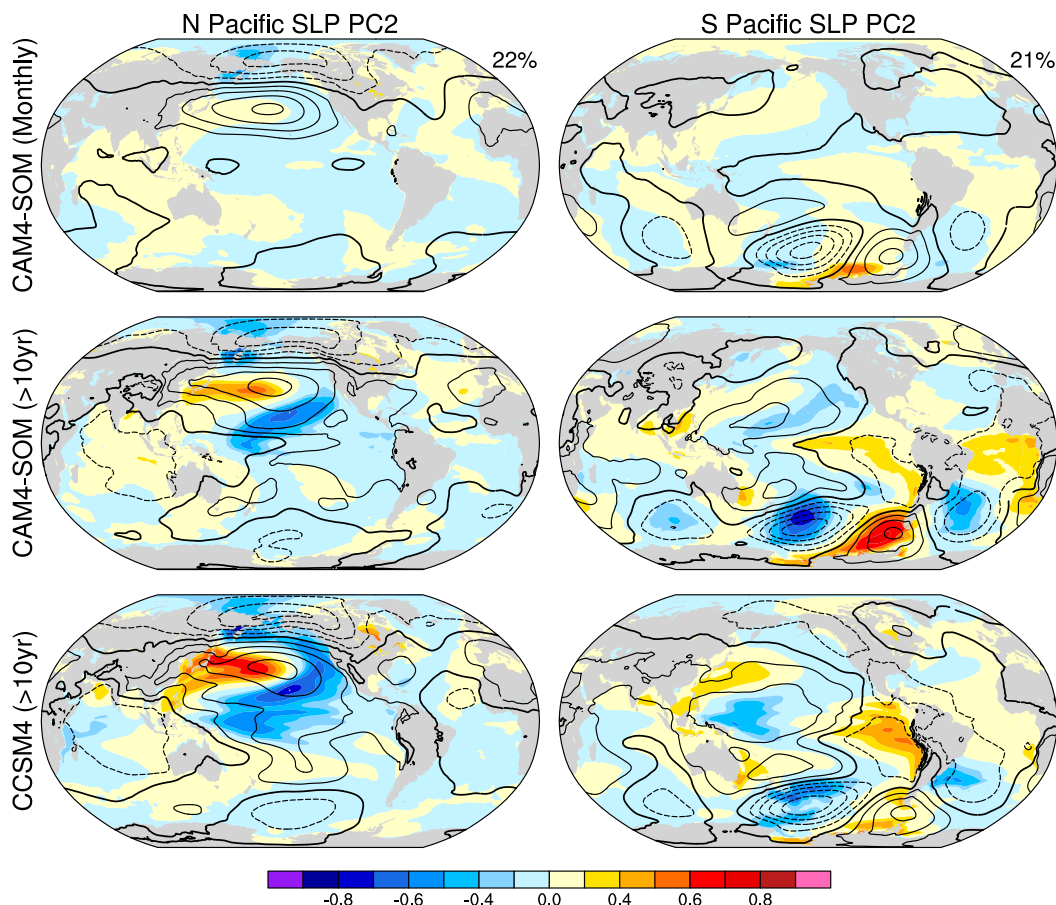


FIG. 19. Correlation maps of global SLP (contours at intervals of 0.2; zero contours thickened) and surface temperature (shading) anomalies with the PC2 of monthly SLP variability over the extratropical (left) North (15° – 70° N, 130° E– 110° W) and (right) South (15° – 70° S, 170° E– 70° W) Pacific in (top), (middle) the CAM4-SOM and (bottom) CCSM4 control simulations. In (middle), (bottom), the monthly PCs and SLP and surface temperature data are smoothed with a 10-yr low-pass filter prior to the correlation analysis. In CAM4-SOM (CCSM4), the North and South Pacific SLP EOF modes explain 22% and 21% (22% and 21%) of the total variance, respectively.

Niño events are likely to shift the background climate of the tropical Pacific more toward El Niño-like state, as suggested by Vimont (2005). During the positive phase of the second TPDV mode, on the other hand, the ocean–atmosphere anomaly patterns become more asymmetric between El Niño and La Niña compared to the negative phase. The sum of El Niño and La Niña composite anomalies produces a residual pattern very similar to changes in the background state during the positive phase of the second TPDV mode, while the asymmetry is negligible during the negative phase (Fig. 20). These changes in the background state induced by ENSO modulation would further enhance changes in ENSO. Indeed, the ENSO amplitude and TPDV PC2 are positively correlated for both positive and negative lags, indicative of their positive feedback (Fig. 21). The correlations are slightly larger when the ENSO amplitude leads TPDV

PC2, suggesting that the ENSO dynamics may play a more important role in generating the distinct zonal dipole pattern of the second TPDV mode than stochastic atmospheric forcing.

5. Summary

The analyses of the 1300-yr CCSM4 control simulation show that various properties of ENSO modulate on decadal–interdecadal time scales in association with the two leading modes of TPDV. In addition to the amplitude, which previous studies of ENSO modulation focus on, we show that the frequency, duration, and pattern of ENSO also exhibit distinct decadal modulation in CCSM4. In particular, the leading mode of TPDV, the simulated IPO, is related to significant changes in the frequency and duration of El Niño events. The relation between the IPO and ENSO

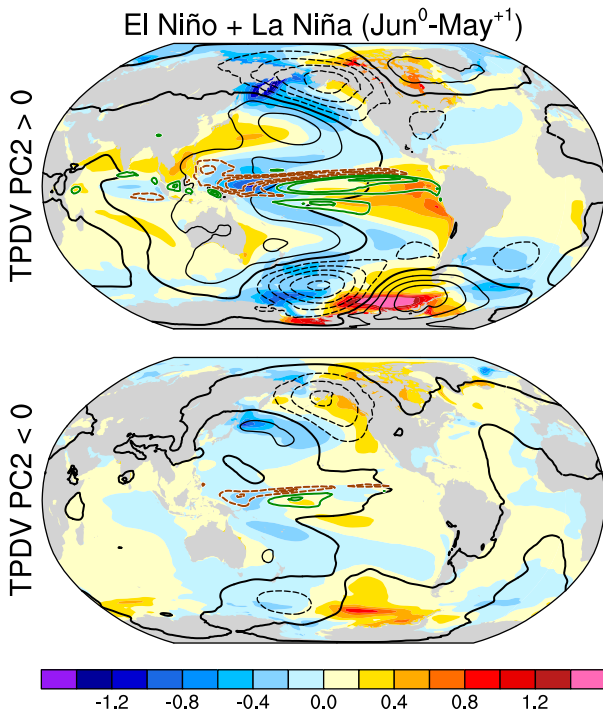


FIG. 20. Sum of El Niño and La Niña composite anomalies of surface temperature ($^{\circ}\text{C}$; shading), SLP (black contours at intervals of 0.5 hPa; zero contours thickened), and precipitation [positive (negative) contours in green solid (brown dashed) at intervals of 1 mm day^{-1}] for $\text{Jun}^0\text{--May}^{+1}$ during the (top) positive and (bottom) negative phases of the second TPDV mode.

modulation remained ambiguous in previous studies, and this result may help us to understand observed ENSO changes associated with IPO. The second leading mode of TPDV, on the other hand, is highly correlated with the ENSO amplitude and duration of La Niña events, as well as the asymmetry in the pattern and duration of El Niño and La Niña. The relation between the second TPDV mode and ENSO amplitude has been known from previous studies, but we show that different processes affect the amplitude of El Niño and La Niña.

The ENSO modulation associated with the two leading modes of TPDV is not symmetrical between El Niño and La Niña and detailed analyses of the modulation mechanisms suggest nonlinear nature of the tropical ocean–atmosphere system. In general, El Niño, which tends to develop from neutral condition, appears more sensitive to decadal changes in the background state. The frequency and duration of El Niño modulate in association with decadal changes in the interbasin SST gradient. Although the same mechanism seems to affect the frequency and duration of La Niña, La Niña is equally influenced by changes in El Niño that often precedes La Niña, and these effects

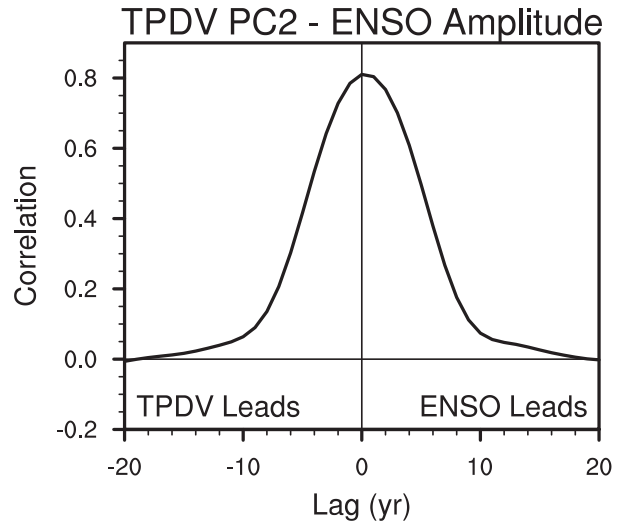


FIG. 21. Lead–lag correlations between the PC2 of TPDV and 10-yr running standard deviation of the Niño-3.4 index (ENSO amplitude). Positive (negative) lags indicate that the ENSO amplitude leads (lags) the TPDV PC2.

tend to cancel each other. The pattern and seasonal evolution of El Niño are also more sensitive to decadal changes in the background state than those of La Niña because of the nonlinear relation between the atmospheric deep convection and SSTs. The resultant changes in the amplitude of El Niño drive changes in the amplitude and duration of the following La Niña.

These asymmetric changes in El Niño and La Niña cannot be simply explained by random forcing and are indicative of the complex and interactive nature of TPDV and ENSO. The comparison of TPDV in the CCSM4 and CAM4-SOM control simulations suggests that TPDV does not require the equatorial ocean dynamics for its presence. Internal atmospheric variability over the South Pacific appears to play an important role in both of the two leading modes of TPDV because of the meridional asymmetry in tropical Pacific climate. The stochastically forced TPDV may modulate the properties of El Niño and the following La Niña, and these ENSO changes would, in turn, positively feed back to TPDV. These hypotheses of TPDV–ENSO interactions are currently being tested with CCSM4 experiments, and the results will be reported in the near future.

Although the CCSM4 simulates many important features of tropical Pacific climate and variability, it remains to be seen to what degree the mechanisms of TPDV and ENSO modulation in CCSM4 apply to the real world. The excessively strong ENSO in this model may affect the strength of interactions between TPDV and ENSO. The comparison of these model results with observations is not trivial, as observational data

are available only for the past 150 yr, which covers only 1–2 cycles of TPDV and ENSO modulation, in addition to the uncertainty in early observations and the difficulty in separating TPDV from anthropogenic effects (e.g., Deser et al. 2010b; Tokinaga et al. 2012). Paleoclimate proxy data from various sources may become useful tools to analyze the relation of TPDV and ENSO modulation (e.g., McGregor et al. 2010, 2013b; Emile-Geay et al. 2013). Nonetheless, the processes that control various properties of El Niño and La Niña analyzed in this study will provide new foundations to further our understanding not only of TPDV and ENSO modulation, but also of seasonal ENSO prediction and anthropogenic ENSO change.

Acknowledgments. The CCSM4 simulation was conducted by the CESM project team and the CAM4-SOM simulation by Robert Tomas. The authors thank Shang-Ping Xie, Clara Deser, and Pedro DiNezio for helpful discussions and Shaikh Muhammad for his assistance with the CAM4 experiments. Comments and suggestions by three anonymous reviewers greatly helped to improve the manuscript. This work is supported by the NSF Climate and Large-Scale Dynamics Program (AGS-1302346) and the NOAA Climate Program Office Modeling, Analysis, Predictions, and Projections Program (NA14OAR4310227).

REFERENCES

- Alexander, M. A., I. Blade, M. Newman, J. R. Lanzante, N.-C. Lau, and J. D. Scott, 2002: The atmospheric bridge: The influence of ENSO teleconnections on air–sea interaction over the global oceans. *J. Climate*, **15**, 2205–2231, doi:10.1175/1520-0442(2002)015<2205:TABTIO>2.0.CO;2.
- , D. J. Vimont, P. Chang, and J. D. Scott, 2010: The impact of extratropical atmospheric variability on ENSO: Testing the seasonal footprinting mechanism using coupled model experiments. *J. Climate*, **23**, 2885–2901, doi:10.1175/2010JCLI3205.1.
- An, S.-I., 2004: Interdecadal changes in the El Niño–La Niña asymmetry. *Geophys. Res. Lett.*, **31**, L23210, doi:10.1029/2004GL021699.
- , and J. Choi, 2015: Why the twenty-first century tropical Pacific trend pattern cannot significantly influence ENSO amplitude? *Climate Dyn.*, **44**, 133–146, doi:10.1007/s00382-014-2233-2.
- Anderson, B. T., 2003: Tropical Pacific sea-surface temperatures and preceding sea level pressure anomalies in the subtropical North Pacific. *J. Geophys. Res.*, **108**, 4732, doi:10.1029/2003JD003805.
- Bailey, D., C. Hannay, M. Holland, and R. Neale, 2009: Slab ocean model forcing. NCAR Tech. Note, 2 pp. [Available online at <http://www.cesm.ucar.edu/models/cesm1.2/data8/doc/SOM.pdf>.]
- Barnett, T., D. Pierce, M. Latif, D. Dommenget, and R. Saravanan, 1999: Interdecadal interactions between tropics and midlatitudes in the Pacific Basin. *Geophys. Res. Lett.*, **26**, 615–618, doi:10.1029/1999GL900042.
- Burgers, G., and D. B. Stephenson, 1999: The “normality” of El Niño. *Geophys. Res. Lett.*, **26**, 1027–1030, doi:10.1029/1999GL900161.
- Burgman, R. J., P. S. Schopf, and B. P. Kirtman, 2008: Decadal modulation of ENSO in a hybrid coupled model. *J. Climate*, **21**, 5482–5500, doi:10.1175/2008JCLI1933.1.
- Cai, W., and Coauthors, 2014: Increasing frequency of extreme El Niño events due to greenhouse warming. *Nat. Climate Change*, **4**, 111–116, doi:10.1038/nclimate2100.
- , and Coauthors, 2015: ENSO and greenhouse warming. *Nat. Climate Change*, **5**, 849–859, doi:10.1038/nclimate2743.
- Chang, P., and Coauthors, 2006: Climate fluctuations of tropical coupled systems—The role of ocean dynamics. *J. Climate*, **19**, 5122–5174, doi:10.1175/JCLI3903.1.
- , L. Zhang, R. Saravanan, D. J. Vimont, J. C. H. Chiang, L. Ji, H. Seidel, and M. K. Tippett, 2007: Pacific meridional mode and El Niño–Southern Oscillation. *Geophys. Res. Lett.*, **34**, L16608, doi:10.1029/2007GL030302.
- Chikamoto, Y., A. Timmermann, and J. J. Luo, 2015: Skilful multi-year predictions of tropical trans-basin climate variability. *Nat. Commun.*, **6**, 6869, doi:10.1038/ncomms7869.
- Choi, J., S.-I. An, B. Dewitte, and W. W. Hsieh, 2009: Interactive feedback between the tropical Pacific decadal oscillation and ENSO in a coupled general circulation model. *J. Climate*, **22**, 6597–6611, doi:10.1175/2009JCLI2782.1.
- , —, and S.-W. Yeh, 2012: Decadal amplitude modulation of two types of ENSO and its relationship with the mean state. *Climate Dyn.*, **38**, 2631–2644, doi:10.1007/s00382-011-1186-y.
- , —, and J.-Y. Yu, 2013: ENSO-like and ENSO-induced tropical Pacific decadal variability in CGCMs. *J. Climate*, **26**, 1485–1501, doi:10.1175/JCLI-D-12-00118.1.
- Chung, C. T. Y., and S. B. Power, 2014: Precipitation response to La Niña and global warming in the Indo-Pacific. *Climate Dyn.*, **43**, 3293–3307, doi:10.1007/s00382-014-2105-9.
- , —, J. M. Arblaster, H. A. Rashid, and G. L. Roff, 2014: Nonlinear precipitation response to El Niño and global warming in the Indo-Pacific. *Climate Dyn.*, **42**, 1837–1856, doi:10.1007/s00382-013-1892-8.
- Clement, A., P. DiNezio, and C. Deser, 2011: Rethinking the ocean’s role in the Southern Oscillation. *J. Climate*, **24**, 4056–4072, doi:10.1175/2011JCLI3973.1.
- Cobb, K. M., C. D. Charles, H. Cheng, and R. L. Edwards, 2003: El Niño/Southern Oscillation and tropical Pacific climate during the last millennium. *Nature*, **424**, 271–276, doi:10.1038/nature01779.
- Collins, M., and Coauthors, 2010: The impact of global warming on the tropical Pacific Ocean and El Niño. *Nat. Geosci.*, **3**, 391–397, doi:10.1038/geo868.
- Danabasoglu, G., S. G. Yeager, Y.-O. Kwon, J. J. Tribbia, A. S. Phillips, and J. W. Hurrell, 2012: Variability of the Atlantic meridional overturning circulation in CCSM4. *J. Climate*, **25**, 5153–5172, doi:10.1175/JCLI-D-11-00463.1.
- D’Arrigo, R., E. R. Cook, R. J. Wilson, R. Allan, and M. E. Mann, 2005: On the variability of ENSO over the past six centuries. *Geophys. Res. Lett.*, **32**, L03711, doi:10.1029/2004GL022055.
- Deser, C., A. S. Phillips, and J. W. Hurrell, 2004: Pacific interdecadal climate variability: Linkages between the tropics and North Pacific during boreal winter since 1900. *J. Climate*, **17**, 3109–3124, doi:10.1175/1520-0442(2004)017<3109:PICVLB>2.0.CO;2.
- , M. A. Alexander, S.-P. Xie, and A. S. Phillips, 2010a: Sea surface temperature variability: Patterns and mechanisms. *Annu. Rev. Mar. Sci.*, **2**, 115–143, doi:10.1146/annurev-marine-120408-151453.

- , A. S. Phillips, and M. A. Alexander, 2010b: Twentieth century tropical sea surface temperature trends revisited. *Geophys. Res. Lett.*, **37**, L10701, doi:10.1029/2010GL043321.
- , and Coauthors, 2012: ENSO and Pacific decadal variability in the Community Climate System Model version 4. *J. Climate*, **25**, 2622–2651, doi:10.1175/JCLI-D-11-00301.1.
- DiNezio, P. N., and C. Deser, 2014: Nonlinear controls on the persistence of La Niña. *J. Climate*, **27**, 7335–7355, doi:10.1175/JCLI-D-14-00033.1.
- , B. P. Kirtman, A. C. Clement, S.-K. Lee, G. A. Vecchi, and A. Wittenberg, 2012: Mean climate controls on the simulated response of ENSO to increasing greenhouse gases. *J. Climate*, **25**, 7399–7420, doi:10.1175/JCLI-D-11-00494.1.
- , C. Deser, Y. Okumura, and A. Karspeck, 2017: Mechanisms controlling the predictability of 2-year La Niña. *Climate Dyn.*, doi:10.1007/s00382-017-3575-3, in press.
- Ding, H., N. S. Keenlyside, and M. Latif, 2012: Impact of the equatorial Atlantic on the El Niño Southern Oscillation. *Climate Dyn.*, **38**, 1965–1972, doi:10.1007/s00382-011-1097-y.
- Dommenget, D., 2010: A slab ocean El Niño. *Geophys. Res. Lett.*, **37**, L20701, doi:10.1029/2010GL044888.
- , and M. Latif, 2008: Generation of hyper climate modes. *Geophys. Res. Lett.*, **35**, L02706, doi:10.1029/2007GL031087.
- , T. Bayr, and C. Frauen, 2013: Analysis of the non-linearity in the pattern and time evolution of El Niño Southern Oscillation. *Climate Dyn.*, **40**, 2825–2847, doi:10.1007/s00382-012-1475-0.
- Dong, B., R. T. Sutton, and A. A. Scaife, 2006: Multidecadal modulation of El Niño–Southern Oscillation (ENSO) variance by Atlantic Ocean sea surface temperatures. *Geophys. Res. Lett.*, **33**, L08705, doi:10.1029/2006GL025766.
- Emile-Geay, J., K. M. Cobb, M. E. Mann, and A. T. Wittenberg, 2013: Estimating central equatorial Pacific SST variability over the past millennium. Part II: Reconstructions and implications. *J. Climate*, **26**, 2329–2352, doi:10.1175/JCLI-D-11-00511.1.
- Fang, Y., J. C. Chiang, and P. Chang, 2008: Variation of mean sea surface temperature and modulation of El Niño–Southern Oscillation variance during the past 150 years. *Geophys. Res. Lett.*, **35**, L14709, doi:10.1029/2008GL033761.
- Fedorov, A. V., and S. G. Philander, 2000: Is El Niño changing? *Science*, **288**, 1997–2002, doi:10.1126/science.288.5473.1997.
- , and —, 2001: A stability analysis of tropical ocean–atmosphere interactions: Bridging measurements and theory for El Niño. *J. Climate*, **14**, 3086–3101, doi:10.1175/1520-0442(2001)014<3086:ASAOTO>2.0.CO;2.
- Flügel, M., and P. Chang, 1999: Stochastically induced climate shift of El Niño–Southern Oscillation phenomenon. *Geophys. Res. Lett.*, **26**, 2473–2476, doi:10.1029/1999GL900550.
- , —, and C. Penland, 2004: The role of stochastic forcing in modulating ENSO predictability. *J. Climate*, **17**, 3125–3140, doi:10.1175/1520-0442(2004)017<3125:TROFSI>2.0.CO;2.
- Frankignoul, C., and K. Hasselmann, 1977: Stochastic climate models. Part II. Application to sea-surface temperature variability and thermocline variability. *Tellus*, **29**, 289–305, doi:10.3402/tellusa.v29i4.11362.
- Galanti, E., E. Tziperman, M. Harrison, A. Rosati, R. Giering, and Z. Sirkes, 2002: The equatorial thermocline outcropping—A seasonal control on the tropical Pacific Ocean–atmosphere instability strength. *J. Climate*, **15**, 2721–2739, doi:10.1175/1520-0442(2002)015<2721:TETOAS>2.0.CO;2.
- Garreaud, R. D., and D. S. Battisti, 1999: Interannual (ENSO) and interdecadal (ENSO-like) variability in the Southern Hemisphere tropospheric circulation. *J. Climate*, **12**, 2113–2123, doi:10.1175/1520-0442(1999)012<2113:IEAIEL>2.0.CO;2.
- Gent, P. R., and Coauthors, 2011: The Community Climate System Model version 4. *J. Climate*, **24**, 4973–4991, doi:10.1175/2011JCLI4083.1.
- Gu, D., and S. G. H. Philander, 1995: Secular changes of annual and interannual variability in the tropics during the past century. *J. Climate*, **8**, 864–876, doi:10.1175/1520-0442(1995)008<0864:SCOAAI>2.0.CO;2.
- , and —, 1997: Interdecadal climate fluctuations that depend on exchanges between the tropics and the extratropics. *Science*, **275**, 805–807, doi:10.1126/science.275.5301.805.
- Guilyardi, E., 2006: El Niño–mean state–seasonal cycle interactions in a multi-model ensemble. *Climate Dyn.*, **26**, 329–348, doi:10.1007/s00382-005-0084-6.
- Hao, Z., J. D. Neelin, and F.-F. Jin, 1993: Nonlinear tropical air–sea interaction in the fast-wave limit. *J. Climate*, **6**, 1523–1544, doi:10.1175/1520-0442(1993)006<1523:NTAIT>2.0.CO;2.
- Hazeleger, W., M. Visbeck, M. Cane, A. Karspeck, and N. Naik, 2001: Decadal upper ocean temperature variability in the tropical and subtropical Pacific. *J. Geophys. Res.*, **106**, 8971–8988, doi:10.1029/2000JC000536.
- Hoerling, M. P., A. Kumar, and M. Zhong, 1997: El Niño, La Niña, and the nonlinearity of their teleconnections. *J. Climate*, **10**, 1769–1786, doi:10.1175/1520-0442(1997)010<1769:ENOLNA>2.0.CO;2.
- Jansen, M. F., D. Dommenget, and N. Keenlyside, 2009: Tropical atmosphere–ocean interactions in a conceptual framework. *J. Climate*, **22**, 550–567, doi:10.1175/2008JCLI2243.1.
- Jin, F.-F., and J. D. Neelin, 1993: Modes of interannual tropical ocean–atmosphere interaction—A unified view. Part I: Numerical results. *J. Atmos. Sci.*, **50**, 3477–3503, doi:10.1175/1520-0469(1993)050<3477:MOITOI>2.0.CO;2.
- , S.-I. An, A. Timmermann, and J. Zhao, 2003: Strong El Niño events and nonlinear dynamical heating. *Geophys. Res. Lett.*, **30**, 1120, doi:10.1029/2002GL016356.
- Kang, I.-S., and J.-S. Kug, 2002: El Niño and La Niña sea surface temperature anomalies: Asymmetry characteristics associated with their wind stress anomalies. *J. Geophys. Res.*, **107**, 4372, doi:10.1029/2001JD000393.
- , H.-H. No, and F. Kucharski, 2014: ENSO amplitude modulation associated with the mean SST changes in the tropical central Pacific induced by Atlantic multidecadal oscillation. *J. Climate*, **27**, 7911–7920, doi:10.1175/JCLI-D-14-00018.1.
- Karspeck, A., and M. A. Cane, 2002: Tropical Pacific 1976–77 climate shift in a linear, wind-driven model. *J. Phys. Oceanogr.*, **32**, 2350–2360, doi:10.1175/1520-0485(2002)032<2350:TPCSIA>2.0.CO;2.
- Kay, J. E., and Coauthors, 2015: The Community Earth System Model (CESM) Large Ensemble Project: A community resource for studying climate change in the presence of internal climate variability. *Bull. Amer. Meteor. Soc.*, **96**, 1333–1349, doi:10.1175/BAMS-D-13-00255.1.
- Kessler, W. S., 2002: Is ENSO a cycle or a series of events? *Geophys. Res. Lett.*, **29**, 2125, doi:10.1029/2002GL015924.
- Kiem, A. S., S. W. Franks, and G. Kuczera, 2003: Multi-decadal variability of flood risk. *Geophys. Res. Lett.*, **30**, 1035, doi:10.1029/2002GL015992.
- Larkin, N. K., and D. E. Harrison, 2002: ENSO warm (El Niño) and cold (La Niña) event life cycles: Ocean surface anomaly patterns, their symmetries, asymmetries, and implications. *J. Climate*, **15**, 1118–1140, doi:10.1175/1520-0442(2002)015<1118:EWENOA>2.0.CO;2.

- Latif, M., and T. P. Barnett, 1995: Interactions of the tropical oceans. *J. Climate*, **8**, 952–964, doi:10.1175/1520-0442(1995)008<0952: IOTTO>2.0.CO;2.
- Li, J., S.-P. Xie, E. R. Cook, G. Huang, R. D'Arrigo, F. Liu, J. Ma, and X.-T. Zheng, 2011: Interdecadal modulation of El Niño amplitude during the past millennium. *Nat. Climate Change*, **1**, 114–118, doi:10.1038/nclimate1086.
- Liu, Z., 2012: Dynamics of interdecadal climate variability: A historical perspective. *J. Climate*, **25**, 1963–1995, doi:10.1175/2011JCLI3980.1.
- Mantua, N. J., S. R. Hare, Y. Zhang, J. M. Wallace, and R. C. Francis, 1997: A Pacific interdecadal climate oscillation with impacts on salmon production. *Bull. Amer. Meteor. Soc.*, **78**, 1069–1079, doi:10.1175/1520-0477(1997)078<1069: APICOW>2.0.CO;2.
- McGregor, S., A. Timmermann, and O. Timm, 2010: A unified proxy for ENSO and PDO variability since 1650. *Climate Past*, **6**, 1–17, doi:10.5194/cp-6-1-2010.
- , N. Ramesh, P. Spence, M. H. England, M. J. McPhaden, and A. Santoso, 2013a: Meridional movement of wind anomalies during ENSO events and their role in event termination. *Geophys. Res. Lett.*, **40**, 749–754, doi:10.1002/grl.50136.
- , A. Timmermann, M. H. England, O. E. Timm, and A. T. Wittenberg, 2013b: Inferred changes in El Niño–Southern Oscillation variance over the past six centuries. *Climate Past*, **9**, 2269–2284, doi:10.5194/cp-9-2269-2013.
- , —, M. F. Stuecker, M. H. England, M. Merrifield, F.-F. Jin, and Y. Chikamoto, 2014: Recent Walker circulation strengthening and Pacific cooling amplified by Atlantic warming. *Nat. Climate Change*, **4**, 888–892, doi:10.1038/nclimate2330.
- McPhaden, M. J., and X. Zhang, 2009: Asymmetry in zonal phase propagation of ENSO sea surface temperature anomalies. *Geophys. Res. Lett.*, **36**, L13703, doi:10.1029/2009GL038774.
- Meinen, C. S., and M. J. McPhaden, 2000: Observations of warm water volume changes in the equatorial Pacific and their relationship to El Niño and La Niña. *J. Climate*, **13**, 3551–3559, doi:10.1175/1520-0442(2000)013<3551: OOWWVC>2.0.CO;2.
- Mo, K. C., 2000: Relationships between low-frequency variability in the Southern Hemisphere and sea surface temperature anomalies. *J. Climate*, **13**, 3599–3610, doi:10.1175/1520-0442(2000)013<3599: RBLFVI>2.0.CO;2.
- Neale, R. B., J. H. Richter, and M. Jochum, 2008: The impact of convection on ENSO: From a delayed oscillator to a series of events. *J. Climate*, **21**, 5904–5924, doi:10.1175/2008JCLI2244.1.
- Neelin, J. D., D. S. Battisti, A. C. Hirst, F.-F. Jin, Y. Wakata, T. Yamagata, and S. E. Zebiak, 1998: ENSO theory. *J. Geophys. Res.*, **103**, 14261–14290, doi:10.1029/97JC03424.
- Newman, M., and Coauthors, 2016: The Pacific decadal oscillation, revisited. *J. Climate*, **29**, 4399–4427, doi:10.1175/JCLI-D-15-0508.1.
- Nitta, T., and S. Yamada, 1989: Recent warming of tropical sea surface temperature and its relationship to the Northern Hemisphere circulation. *J. Meteor. Soc. Japan*, **67**, 375–383, doi:10.2151/jmsj1965.67.3_375.
- Ogata, T., S.-P. Xie, A. Wittenberg, and D.-Z. Sun, 2013: Interdecadal amplitude modulation of El Niño–Southern Oscillation and its impact on tropical Pacific decadal variability. *J. Climate*, **26**, 7280–7297, doi:10.1175/JCLI-D-12-00415.1.
- Ohba, M., and H. Ueda, 2009: Role of nonlinear atmospheric response to SST on the asymmetric transition process of ENSO. *J. Climate*, **22**, 177–192, doi:10.1175/2008JCLI2334.1.
- , and M. Watanabe, 2012: Role of the Indo-Pacific interbasin coupling in predicting asymmetric ENSO transition and duration. *J. Climate*, **25**, 3321–3335, doi:10.1175/JCLI-D-11-00409.1.
- Okumura, Y. M., 2013: Origins of tropical Pacific decadal variability: Role of stochastic atmospheric forcing from the South Pacific. *J. Climate*, **26**, 9791–9796, doi:10.1175/JCLI-D-13-00448.1.
- , and C. Deser, 2010: Asymmetry in the duration of El Niño and La Niña. *J. Climate*, **23**, 5826–5843, doi:10.1175/2010JCLI3592.1.
- , M. Ohba, C. Deser, and H. Ueda, 2011: A proposed mechanism for the asymmetric duration of El Niño and La Niña. *J. Climate*, **24**, 3822–3829, doi:10.1175/2011JCLI3999.1.
- Pierce, D., T. Barnett, and M. Latif, 2000: Connections between the Pacific Ocean tropics and midlatitudes on decadal timescales. *J. Climate*, **13**, 1173–1194, doi:10.1175/1520-0442(2000)013<1173: CBTPOT>2.0.CO;2.
- Power, S., T. Casey, C. Folland, A. Colman, and V. Mehta, 1999: Inter-decadal modulation of the impact of ENSO on Australia. *Climate Dyn.*, **15**, 319–324, doi:10.1007/s003820050284.
- , M. Haylock, R. Colman, and X. Wang, 2006: The predictability of interdecadal changes in ENSO activity and ENSO teleconnections. *J. Climate*, **19**, 4755–4771, doi:10.1175/JCLI3868.1.
- Rayner, N. A., D. E. Parker, E. B. Horton, C. K. Folland, L. V. Alexander, D. P. Rowell, E. C. Kent, and A. Kaplan, 2003: Global analyses of sea surface temperature, sea ice, and night marine air temperature since the late nineteenth century. *J. Geophys. Res.*, **108**, 4407, doi:10.1029/2002JD002670.
- Rodgers, K. B., P. Friederichs, and M. Latif, 2004: Tropical Pacific decadal variability and its relation to decadal modulations of ENSO. *J. Climate*, **17**, 3761–3774, doi:10.1175/1520-0442(2004)017<3761:TPDVAI>2.0.CO;2.
- Rogers, J. C., 1981: The North Pacific Oscillation. *J. Climatol.*, **1**, 39–52, doi:10.1002/joc.3370010106.
- Schneider, N., A. Miller, M. Alexander, C. Deser, and M. Latif, 1999a: Subduction of decadal North Pacific temperature anomalies: Observations and dynamics. *J. Phys. Oceanogr.*, **29**, 1056–1070, doi:10.1175/1520-0485(1999)029<1056: SODNPT>2.0.CO;2.
- , S. Venzke, A. Miller, D. Pierce, T. Barnett, C. Deser, and M. Latif, 1999b: Pacific thermocline bridge revisited. *Geophys. Res. Lett.*, **26**, 1329–1332, doi:10.1029/1999GL900222.
- Schopf, P. S., and R. J. Burgman, 2006: A simple mechanism for ENSO residuals and asymmetry. *J. Climate*, **19**, 3167–3179, doi:10.1175/JCLI3765.1.
- Schott, F. A., S.-P. Xie, and J. P. McCreary, 2009: Indian Ocean circulation and climate variability. *Rev. Geophys.*, **47**, RG1002, doi:10.1029/2007RG000245.
- Sun, D.-Z., and T. Zhang, 2006: A regulatory effect of ENSO on the time-mean thermal stratification of the equatorial upper ocean. *Geophys. Res. Lett.*, **33**, L07710, doi:10.1029/2005GL025384.
- Sun, F., and J.-Y. Yu, 2009: A 10–15-yr modulation cycle of ENSO intensity. *J. Climate*, **22**, 1718–1735, doi:10.1175/2008JCLI2285.1.
- Takahashi, K., and B. Dewitte, 2016: Strong and moderate nonlinear El Niño regimes. *Climate Dyn.*, **46**, 1627–1645, doi:10.1007/s00382-015-2665-3.
- Thompson, C. J., and D. S. Battisti, 2001: A linear stochastic dynamical model of ENSO. Part II: Analysis. *J. Climate*, **14**, 445–466, doi:10.1175/1520-0442(2001)014<0445:ALSDMO>2.0.CO;2.
- Timmermann, A., 2003: Decadal ENSO amplitude modulations: A nonlinear paradigm. *Global Planet. Change*, **37**, 135–156, doi:10.1016/S0921-8181(02)00194-7.

- , and Coauthors, 2007: The influence of a weakening of the Atlantic meridional overturning circulation on ENSO. *J. Climate*, **20**, 4899–4919, doi:[10.1175/JCLI4283.1](https://doi.org/10.1175/JCLI4283.1).
- Tokinaga, H., S.-P. Xie, C. Deser, Y. Kosaka, and Y. M. Okumura, 2012: Slowdown of the Walker circulation driven by tropical Indo-Pacific warming. *Nature*, **491**, 439–443, doi:[10.1038/nature11576](https://doi.org/10.1038/nature11576).
- Trenberth, K. E., and D. J. Shea, 1987: On the evolution of the Southern Oscillation. *Mon. Wea. Rev.*, **115**, 3078–3096, doi:[10.1175/1520-0493\(1987\)115<3078:OTEOTS>2.0.CO;2](https://doi.org/10.1175/1520-0493(1987)115<3078:OTEOTS>2.0.CO;2).
- , and J. W. Hurrell, 1994: Decadal atmosphere–ocean variations in the Pacific. *Climate Dyn.*, **9**, 303–319, doi:[10.1007/BF00204745](https://doi.org/10.1007/BF00204745).
- , G. W. Branstator, D. Karoly, A. Kumar, N.-C. Lau, and C. Ropelewski, 1998: Progress during TOGA in understanding and modeling global teleconnections associated with tropical sea surface temperatures. *J. Geophys. Res.*, **103**, 14 291–14 324, doi:[10.1029/97JC01444](https://doi.org/10.1029/97JC01444).
- Verdon, D. C., and S. W. Franks, 2006: Long-term behavior of ENSO: Interactions with the PDO over the past 400 years inferred from paleoclimate records. *Geophys. Res. Lett.*, **33**, L06712, doi:[10.1029/2005GL025052](https://doi.org/10.1029/2005GL025052).
- Vimont, D. J., 2005: The contribution of the interannual ENSO cycle to the spatial pattern of decadal ENSO-like variability. *J. Climate*, **18**, 2080–2092, doi:[10.1175/JCLI3365.1](https://doi.org/10.1175/JCLI3365.1).
- , D. S. Battisti, and A. C. Hirst, 2001: Footprinting: A seasonal connection between the tropics and mid-latitudes. *Geophys. Res. Lett.*, **28**, 3923–3926, doi:[10.1029/2001GL013435](https://doi.org/10.1029/2001GL013435).
- Wallace, J. M., E. M. Rasmusson, T. P. Mitchell, V. E. Kousky, E. S. Sarachik, and H. von Storch, 1998: On the structure and evolution of ENSO-related climate variability in the tropical Pacific: Lessons from TOGA. *J. Geophys. Res.*, **103**, 14 241–14 259, doi:[10.1029/97JC02905](https://doi.org/10.1029/97JC02905).
- Wang, B., and Y. Wang, 1996: Temporal structure of the Southern Oscillation as revealed by waveform and wavelet analysis. *J. Climate*, **9**, 1586–1598, doi:[10.1175/1520-0442\(1996\)009<1586:TSOTSO>2.0.CO;2](https://doi.org/10.1175/1520-0442(1996)009<1586:TSOTSO>2.0.CO;2).
- , and S.-I. An, 2002: A mechanism for decadal changes of ENSO behavior: Roles of background wind changes. *Climate Dyn.*, **18**, 475–486, doi:[10.1007/s00382-001-0189-5](https://doi.org/10.1007/s00382-001-0189-5).
- Wang, C., 2006: An overlooked feature of tropical climate: Inter-Pacific–Atlantic variability. *Geophys. Res. Lett.*, **33**, L12702, doi:[10.1029/2006GL026324](https://doi.org/10.1029/2006GL026324).
- , and J. Picaut, 2004: Understanding ENSO physics—A review. *Earth's Climate: The Ocean–Atmosphere Interaction, Geophys. Monogr.*, Vol. 147, Amer. Geophys. Union, 21–48, doi:[10.1029/147GM02](https://doi.org/10.1029/147GM02).
- Wittenberg, A. T., A. Rosati, T. L. Delworth, G. A. Vecchi, and F. Zeng, 2014: ENSO modulation: Is it decadalily predictable? *J. Climate*, **27**, 2667–2681, doi:[10.1175/JCLI-D-13-00577.1](https://doi.org/10.1175/JCLI-D-13-00577.1).
- Wu, A., and W. W. Hsieh, 2003: Nonlinear interdecadal changes of the El Niño–Southern Oscillation. *Climate Dyn.*, **21**, 719–730, doi:[10.1007/s00382-003-0361-1](https://doi.org/10.1007/s00382-003-0361-1).
- Wu, B., T. Li, and T. Zhou, 2010: Asymmetry of atmospheric circulation anomalies over the western North Pacific between El Niño and La Niña. *J. Climate*, **23**, 4807–4822, doi:[10.1175/2010JCLI3222.1](https://doi.org/10.1175/2010JCLI3222.1).
- Xie, S.-P., and J. A. Carton, 2004: Tropical Atlantic variability: Patterns, mechanisms, and impacts. *Earth Climate: The Ocean–Atmosphere Interaction, Geophys. Monogr.*, Vol. 147, Amer. Geophys. Union, 121–142, doi:[10.1029/147GM07](https://doi.org/10.1029/147GM07).
- Ye, Z., and W. W. Hsieh, 2006: The influence of climate regime shift on ENSO. *Climate Dyn.*, **26**, 823–833, doi:[10.1007/s00382-005-0105-5](https://doi.org/10.1007/s00382-005-0105-5).
- Yeh, S.-W., and B. P. Kirtman, 2004: Tropical Pacific decadal variability and ENSO amplitude modulation in a CGCM. *J. Geophys. Res.*, **109**, C11009, doi:[10.1029/2004JC002442](https://doi.org/10.1029/2004JC002442).
- , and —, 2005: Pacific decadal variability and decadal ENSO amplitude modulation. *Geophys. Res. Lett.*, **32**, L05703, doi:[10.1029/2004GL021731](https://doi.org/10.1029/2004GL021731).
- , J.-G. Jhun, I.-S. Kang, and B. P. Kirtman, 2004: The decadal ENSO variability in a hybrid coupled model. *J. Climate*, **17**, 1225–1238, doi:[10.1175/1520-0442\(2004\)017<1225:TDEVIA>2.0.CO;2](https://doi.org/10.1175/1520-0442(2004)017<1225:TDEVIA>2.0.CO;2).
- Zhang, H., A. Clement, and P. DiNezio, 2014a: The South Pacific meridional mode: A mechanism for ENSO-like variability. *J. Climate*, **27**, 769–783, doi:[10.1175/JCLI-D-13-00082.1](https://doi.org/10.1175/JCLI-D-13-00082.1).
- , C. Deser, A. Clement, and R. Tomas, 2014b: Equatorial signatures of the Pacific meridional modes: Dependence on mean climate state. *Geophys. Res. Lett.*, **41**, 568–574, doi:[10.1002/2013GL058842](https://doi.org/10.1002/2013GL058842).
- Zhang, R.-H., L. M. Rothstein, and A. J. Busalacchi, 1998: Origin of upper-ocean warming and El Niño change on decadal scales in the tropical Pacific Ocean. *Nature*, **391**, 879–883, doi:[10.1038/36081](https://doi.org/10.1038/36081).
- Zhang, Y., J. M. Wallace, and D. S. Battisti, 1997: ENSO-like interdecadal variability: 1900–93. *J. Climate*, **10**, 1004–1020, doi:[10.1175/1520-0442\(1997\)010<1004:ELIV>2.0.CO;2](https://doi.org/10.1175/1520-0442(1997)010<1004:ELIV>2.0.CO;2).
- Zheng, X.-T., S.-P. Xie, L.-H. Lv, and Z.-Q. Zhou, 2016: Intermodel uncertainty in ENSO amplitude change tied to Pacific Ocean warming pattern. *J. Climate*, **29**, 7265–7279, doi:[10.1175/JCLI-D-16-0039.1](https://doi.org/10.1175/JCLI-D-16-0039.1).